



Lawrence Berkeley Laboratory

UNIVERSITY OF CALIFORNIA

RECEIVED
LAWRENCE
BERKELEY LABORATORY

Materials & Molecular Research Division

JUN 18 1982

LIBRARY AND
DOCUMENTS SECTION

HEAT CAPACITY OF α -CE BETWEEN 0.3 AND 20K AT
PRESSURES TO 9.0KBAR AND MAGNETIC FIELDS TO 7.5T

James D. Boyer
(Ph.D. thesis)

May 1982

TWO-WEEK LOAN COPY

*This is a Library Circulating Copy
which may be borrowed for two weeks.
For a personal retention copy, call
Tech. Info. Division, Ext. 6782.*



LBL-13645
c. 2

DISCLAIMER

This document was prepared as an account of work sponsored by the United States Government. While this document is believed to contain correct information, neither the United States Government nor any agency thereof, nor the Regents of the University of California, nor any of their employees, makes any warranty, express or implied, or assumes any legal responsibility for the accuracy, completeness, or usefulness of any information, apparatus, product, or process disclosed, or represents that its use would not infringe privately owned rights. Reference herein to any specific commercial product, process, or service by its trade name, trademark, manufacturer, or otherwise, does not necessarily constitute or imply its endorsement, recommendation, or favoring by the United States Government or any agency thereof, or the Regents of the University of California. The views and opinions of authors expressed herein do not necessarily state or reflect those of the United States Government or any agency thereof or the Regents of the University of California.

LBL-13645

HEAT CAPACITY OF α -CE BETWEEN 0.3 AND 20K
AT PRESSURES TO 9.0KBAR AND MAGNETIC FIELDS TO 7.5T

James D. Boyer

Materials and Molecular Research Division
Lawrence Berkeley Laboratory and Department of Chemistry
University of California
Berkeley, California

This work was supported by the Director, Office of Energy Research,
Office of Health and Environmental Research of the U.S. Department of
Energy under Contract No. DE-AC03-76SF00098.

Contents

ABSTRACT	v
--------------------	---

PART ONE: PRESSURE DEPENDENCE OF THE LOW-TEMPERATURESPECIFIC HEAT OF α -CERIUM

I. INTRODUCTION	1
II. EXPERIMENTAL TECHNIQUES.	11
A. Thermometry.	11
B. Cryostat	11
C. Calorimeters	12
D. Pressure Cell.	13
E. Pressure Transmitting Medium	15
F. Pressure Measurement	16
G. Samples.	17
H. Pressurization	18
J. Addenda Heat Capacity.	20
III. RESULTS AND ANALYSIS	22
A. Heat Capacity Experiments.	22
B. Data Analysis Technique.	24
C. β -Cerium Contributions	31
D. Anomalous Low-Temperature Contributions.	33
E. Pressure Dependence.	36
F. Thermal Expansion Coefficient.	40
G. Magnetic Field Dependence.	45

IV. DISCUSSION	48
REFERENCES	61

PART TWO: A SEMI-AUTOMATIC LOW-TEMPERATURE CALORIMETRY SYSTEM

I. INTRODUCTION	65
II. CALORIMETRY.	69
III. TEMPERATURE MEASUREMENT SYSTEM	71
IV. ENERGY CONTROL AND MEASUREMENT SYSTEM.	77
V. THE COMPUTER AND OPERATING SYSTEM.	80
VI. COMMAND CODE DESCRIPTIONS.	88
A. Definitions.	88
B. Data Entry Command Codes	88
C. Process Control Command Codes.	89
D. Computation Command Codes.	91
E. Data Output Command Codes.	92
F. Miscellaneous Command Codes.	93
VII. SYSTEM PERFORMANCE	94
REFERENCES	96

PART THREE: PRESSURE DEPENDENCE OF THE LOW-TEMPERATURE

SPECIFIC HEAT OF TEFLON

I. INTRODUCTION	97
II. RESULTS AND DISCUSSION	99
REFERENCES	111
ACKNOWLEDGMENTS.	112

PART ONE: THE PRESSURE DEPENDENCE OF THE LOW-TEMPERATURE HEAT
CAPACITY OF α -CERIUM

PART TWO: A SEMI-AUTOMATIC LOW-TEMPERATURE CALORIMETRY SYSTEM

PART THREE: THE PRESSURE DEPENDENCE OF THE LOW-TEMPERATURE
HEAT CAPACITY OF TEFLON

JAMES D. BOYER

Materials and Molecular Research Division
Lawrence Berkeley Laboratory and Department of Chemistry
University of California
Berkeley, California

ABSTRACT

PART ONE: THE PRESSURE DEPENDENCE OF THE LOW-TEMPERATURE
HEAT CAPACITY OF α -CERIUM

The heat capacity of α -cerium was measured at pressures from 2.3 to 9.0kbar for temperatures 0.3–20K and at 5.2kbar for temperatures of 1.3–4.2K in magnetic fields to 7.5T. The volume dependences of the electronic specific heat coefficient, γ , and the Debye temperature were determined. The volume dependence of γ is well described by several promotional models for the cerium γ - α phase transition. Agreement with band-structure calculations is obtained only by assuming a volume dependent spin-fluctuation enhancement, λ_{sf} , to the electron effective mass. The same λ_{sf} , which decreases with volume, could explain the volume dependence of the superconducting transition temperature in α -cerium. The thermal expansion coefficient, $\beta = V^{-1} (\partial V / \partial T)_p$, was calculated from the pressure dependence of the entropy for 0.3–20K.

PART TWO: A SEMI-AUTOMATIC LOW-TEMPERATURE CALORIMETRY SYSTEM

The design and operation of a microcomputer based low-temperature calorimetry system is described. The system features interactive data acquisition and on-line data reduction. In addition to increased experimental efficiency, improvements in the precision of heat capacity were obtained.

PART THREE: THE PRESSURE DEPENDENCE OF THE LOW-TEMPERATURE HEAT CAPACITY OF TEFLON

The heat capacity, C_v , of a teflon sample was measured at pressures from 0.3 to 5.2kbar for temperatures 0.7-20K. The pressure dependence of C_v is large and varies strongly with temperature. The data are well described by a Tarasov term plus two Einstein heat capacity functions. The Einstein terms involve only a small fraction of the total number of vibrational modes, but account for more than 50 percent of the pressure dependence of C_v . On the basis of the data reported here and literature data for other amorphous organic polymers, it is concluded that vibrations associated with side groups are not responsible for the Einstein contributions to C_v .

PART ONE: PRESSURE DEPENDENCE OF THE
LOW-TEMPERATURE SPECIFIC HEAT OF α -CERIUM

I. INTRODUCTION

Metallic cerium, for which the 4f, 5d, and 6s electronic levels are close in energy, exhibits an unusual diversity of behavior in its physical properties. The following discussion highlights these properties. A more detailed discussion and list of references are available in the comprehensive review by Koskenmaki and Gschneidner.¹ Figure 1, the pressure-temperature phase diagram of cerium, shows five solid phases and a critical point. Two of the cerium allotropes, the face centered cubic (fcc), γ phase, and the double hexagonal close-packed (dhcp), β phase, with atomic moments consistent with a singly occupied 4f level, are magnetic. The β phase orders antiferromagnetically at 12.5 and 13.0K with the different ordering temperatures presumably associated with separate ordering at the two different symmetry sites in the dhcp lattice. The other magnetic phase, γ -cerium, does not order at the temperatures for which it is stable. A second fcc phase, α -cerium, is nonmagnetic, but has a strongly enhanced paramagnetic susceptibility. Two of the cerium allotropes, α -cerium and α' -cerium (which is stable at high pressures and is thought to have the α -uranium structure), show superconducting transitions. In α -cerium, however, the transition has only been observed at pressures above 20kbar, at which pressure the transition temperature is only 20mK, despite the high density of states implied by a very large electronic specific heat.

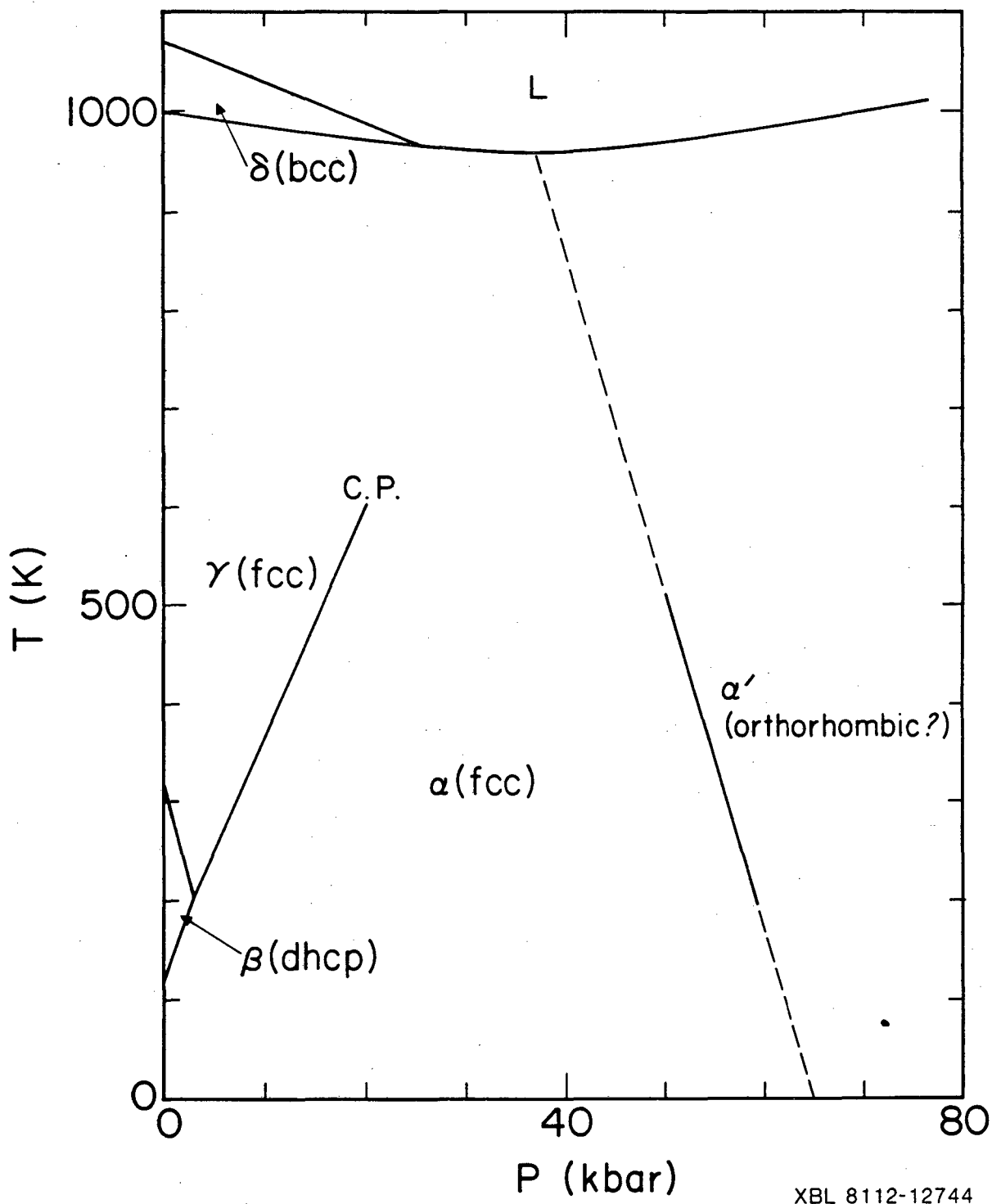


Fig. 1. The temperature pressure phase diagram of cerium.

Much of the experimental and theoretical work on cerium has focused on obtaining an understanding of the two fcc phases and the isomorphic phase transition. The less dense of these, γ -cerium, is stable at higher temperatures and lower pressures than α -cerium. The γ - α phase boundary terminates at a critical point near 600K and 20kbar. At pressures below about 3kbar, the two fcc phases are separated by a region of stability for the dhcp β -cerium. At low pressures the cerium phase transitions are sluggish and do not go to completion. The resulting allotropic mixtures of varying composition are no doubt responsible for the often conflicting experimental results obtained by different investigators. The γ - α transition, near 7.5kbar at ambient temperature, is accompanied by a 17 percent decrease in atomic volume, the disappearance of the γ -cerium local moment, and an abrupt drop in electrical resistivity and Hall coefficient. The transition (which can occur continuously via a path around the critical point) is believed to result from a change in the nature of the cerium 4f electron. Several models have been proposed to account for this transition and are compared with experiment in reference 1.

Most models of the γ - α transition are based on the promotion of a localized 4f electron in γ -cerium into the sd conduction bands as suggested independently by Zachariasen² and Pauling.³ Comparison of the atomic radii of cerium and neighboring elements in the periodic table suggests nonintegral valences for the cerium allotropes and only partial transfer of the 4f electron in the γ - α transition.⁴

The promotional picture receives support from several more detailed theoretical models that account for the significant features of the transition, including the enhanced paramagnetic susceptibility and electronic specific heat of α -cerium. Coqblin and Blandin proposed a virtual bound state model for the γ - α transition in which the tightly bound 4f electrons are treated in the same way as in the isolated impurity problem.⁵ The essential feature of this model is the existence of separate narrow spin-up and spin-down 4f virtual bound states (VBS) lying about 0.1 eV above and below the Fermi level in γ -cerium. Under compression or decreasing temperature, the occupied 4f VBS's coalesce into a single nonmagnetic VBS with a low energy tail extending below the Fermi level. The 4f occupation is determined by the width and position of the VBS relative to the Fermi level and decreases as the VBS rises with increasing pressure or decreasing temperature. The 4f contribution to the electronic density of states accounts for an enhanced paramagnetic susceptibility and electronic specific heat in α -cerium. Another model, proposed by Ramirez and Falicov, supposes the existence of localized magnetic 4f states lying a few tenths of an electron volt above the Fermi level.⁶ The occupation of the localized 4f state is stabilized by an explicit screening interaction G between the 4f states and the conduction electrons and holes that acts to lower the free energy. Minimizing the free energy results in a temperature dependent 4f occupation leading to a first order phase transition with a critical point for suitable choices of the 4f energy level and interaction energy G . While this simplified model does show

a first order transition with a critical point and accounts for the loss of magnetic moment it fails to predict nonintegral valence or the enhanced low-temperature magnetic susceptibility and electronic specific heat. Alascio, Lopez, and Olmedo extended this model by introducing hybridization of the 4f states with the conduction bands.⁷ Hybridization adds a finite 4f occupancy at zero temperature and accounts for fractional valence and enhanced magnetic susceptibility and electronic specific heat in α -cerium. The interconfigurational fluctuation model of Hirst provides a somewhat different promotional picture of the γ - α transition.⁹ For cerium the excitation energy, E , necessary to go from the $4f^1$ to the $4f^0$ configuration, is expected to change from positive to negative as the atomic volume decreases. When E has a value near zero, rapid interconfigurational fluctuations occur. By parametrizing the electronic and elastic energy with the atomic volume, Hirst shows that a discontinuous pressure-volume relation is favored. Furthermore, for a reasonable volume dependence in the elastic energy, E can lock to the value zero resulting in a stable interconfigurational fluctuation (ICF) state. The ICF state exhibits fractional valence and acts as a narrow band at low temperatures and frequencies accounting for the enhanced magnetic susceptibility and electronic specific heat of α -cerium.

Arguments against the promotional picture of the γ - α transition are of both theoretical and experimental origin. For example, both ultraviolet and X-ray photoemission experiments place the 4f level near 1.9eV below the Fermi level in γ -cerium.⁹ If this is correct,

then the energy necessary to lift the 4f level to the Fermi level is much greater than the elastic work needed to compress γ -cerium to α -cerium at room temperature.¹ It has, however, been pointed out that the 4f peak at 1.9eV is relative to a relaxed final state of the system rather than the initial unperturbed state. Consequently, the 4f energy relative to the Fermi level will be somewhat smaller than 1.9eV. Brewer compares the energies of the lowest electronic configurations without 4f electrons to that of cerium metal and concludes that the energy gained due to the greater bonding of a 5d electron relative to a 4f electron is too small to balance the energy necessary for promotion to the lowest non f bonding configuration.¹⁰ A second criticism of the promotional models comes from positron annihilation lifetime and angular correlation experiments.^{11,12} The experimental results show smaller differences between γ and α -cerium than would be expected for a valence change at the transition. Another experimental argument against the promotion models comes from comparison of the experimental Compton profile differences for γ and α -cerium¹³ with those calculated theoretically.^{13,14} Assuming the electronic configuration remains the same in the two phases results in a calculated Compton profile difference in excellent agreement with experiment, whereas assuming even partial transfer of the 4f electron contradicts the experimental difference. On the basis of spectroscopic data and cohesive energy arguments, Johansson suggests that the γ - α transition is a Mott transition within the cerium 4f bands.¹⁵ This viewpoint also agrees with most experimental work with the exception of X-ray

emission and absorption¹⁶ and neutron scattering experiments.¹⁷⁻¹⁹ Support for the Mott transition picture is obtained from recent state of the art band-structure calculations. Glötzel calculates a 4f occupancy of 1.2 for α -cerium and observes a tendency to form a ferromagnetic state as the lattice constants approaches that of γ -cerium.²⁰ The calculations, furthermore, indicate that a 4f contribution to bonding is important in determining the equilibrium atomic radius. Pickett, Freeman, and Koelling examined the γ - α transition with band-structure calculations and found a 4f occupancy increasing from 1.0 to 1.1 in going from γ to α -cerium.²¹ These authors present arguments based on the calculated behavior of the f-bands, reconciling the large body of experimental data with the Mott transition viewpoint. While some recent work lends support to the Mott transition picture of the γ - α transition, there are as yet insufficient data to achieve a general consensus as to which model best represents the γ - α cerium phase transition.

The recent calculations of Glötzel²⁰ and Pickett et al.²¹ produced theoretical estimates of the electronic density of states at the Fermi level, $N(E_F)$, and the electron-phonon enhancement, λ_{ep} , of the electron effective mass. The calculations of Glotzel were for α -cerium at a lattice constant corresponding to zero pressure and his $N(E_F)$ is about 40 percent larger than that obtained by Pickett et al. who suggest that the discrepancy can be accounted for by the slightly different placements of the f-band position relative to E_F . The calculations of Pickett et al., however, provide $N(E_F)$'s at lattice

constants slightly larger than that of α -cerium at zero pressure and at lattice constants appropriate to 15kbar pressure. These are useful in separating the volume dependent contributions to the electronic specific heat coefficient obtained from low-temperature heat capacity measurements on α -cerium as a function of pressure.

Several investigators have attempted to determine the specific heat of α -cerium; however, early measurements were on mixed-phase samples containing varying amounts of the antiferromagnetic β phase.²²⁻²⁴ The large magnetic heat capacity associated with antiferromagnetic ordering of β -cerium dominates the measured heat capacity and leads to large uncertainties in the results for α -cerium. Single-phase cerium samples, now available for experiments through careful heat and pressure treatment,²⁵ yield more meaningful experimental results. The first heat capacity measurement of allotropically pure α -cerium was that of Phillips, Ho, and Smith at 11kbar, for which an electronic specific heat coefficient, γ , of 11.3 mJ/mole-K² and a Debye temperature, θ_0 of 200K, were obtained.²⁶ In a later experiment, Koskimaki and Gschneidner obtained allotropically pure α -cerium at zero pressure and low temperature and determined a γ of 12.8 mJ/mole-K² and a θ_0 of 179K.²⁷ The latter two experiments have been used to infer the pressure dependence of γ and θ_0 for comparison with theory.²¹ The resultant pressure dependence has substantial uncertainty as the experiments were on samples of differing atomic purity and are on different temperature scales; moreover, the 11kbar γ and θ_0 have relatively large experimental uncertainties. In that experiment the

cerium sample contributed only a few percent of the total measured heat capacity. The resulting scatter in the data, which ranged from about 10 percent to as much as 30 percent at the lowest temperatures, not only introduced substantial uncertainty in separation of the electronic and lattice contributions to the heat capacity, but also may have masked low temperature impurity contributions to the heat capacity and led to an overestimate of γ and θ_0 . A more reliable determination of the pressure dependence of the low temperature specific heat of α -cerium, or its volume dependence by use of the cerium pressure-volume relations,²⁸ would provide a better test of the theoretical volume dependence of the electronic specific heat coefficient. The volume dependence of the Debye temperature, θ_0 , which would be obtained from the same experiment, is useful in estimating the mean-square phonon frequency important in determining the electron-phonon enhancement to the electron effective mass. The latter plays an important role in superconductivity and in the electronic specific heat, both of which must be well described by any adequate theory of the γ - α cerium phase transition.

Several techniques have been used for heat capacity measurements at high pressures. One is the quasi-adiabatic heat pulse technique where the temperature change produced by introduction of a known quantity of energy is measured. The ratio of the energy input to the observed temperature change, when corrected for addenda heat capacities and the finite temperature increments, yields the sample heat capacity. High pressures are obtained by compressing the sample within a locking

piston-cylinder pressure cell. The large mechanical stresses present at high pressures require a pressure-cell of relatively massive construction. Consequently, the pressure cell contributes a dominant fraction of the total measured heat capacity and significantly limits obtainable resolution and accuracy. Itskevich, Kraidenov, and Syzranov²⁹ and Eichler and Gey³⁰ have applied the ac calorimetric technique developed by Sullivan and Seidel³¹ to heat capacity measurements at high pressure. While the ac method avoids measurement of the pressure-cell heat capacity and achieves excellent resolution, the technique does not directly determine absolute heat capacity. In special cases, where thermal time constants are favorable, absolute accuracies of several percent can be obtained by use of frequency dependent corrections. For many substances, characterized by high thermal diffusivity, ac calorimetry will probably produce superior high pressure heat capacity results. The heat capacity of α -cerium, however, is large and it is possible to design an experiment where the heat capacity of the pressure-cell relative to that of the sample is such that an accuracy of about one percent is obtainable. For this reason the quasi-adiabatic heat pulse technique was chosen for the measurement of the pressure dependence of the heat capacity of α -cerium.

II. EXPERIMENTAL TECHNIQUES

A. Thermometry

Temperatures were determined by four-lead dc potentiometric resistance measurements of calibrated germanium sensors. Two different germanium thermometers were used. The thermometer designated GE2347 was attached to the calorimeter used in measuring heat capacity versus pressure while the thermometer designated GE1609 was attached to the calorimeter designed for heat capacity measurements in large magnetic fields. Both were calibrated by comparison with the laboratory working temperature scale, T_n , which is preserved on two other germanium sensors permanently mounted in a dedicated calibration apparatus. This scale is based on the NBS platinum resistance scale, T_{55} , for $15 < T < 25\text{K}$, gas thermometry for $4.2 < T < 20\text{K}$, the ^4He vapor pressure scale, T_{52} , for $1.2 < T < 4.2\text{K}$, the He^3 vapor pressure scale, T_{62} , for $1.2 < T < 2.1\text{K}$, and on a CMN magnetic thermometer extrapolation to 0.3K . Conway describes the details of T_n and its establishment more thoroughly in Reference 24.

B. Cryostat

The heat capacity of cerium was measured in a ^3He cryostat described in detail by Senozan³² and Triplett.³³ The vacuum can was modified to seal with an indium O-ring facilitating removal of the pressure cell when changing pressure. The calorimeter is suspended, by nylon threads, from a brass cage attached to a small ^3He pot. Two mechanical heat switches are used. One connects the calorimeter to the

³He pot and the other connects the ³He pot to the ⁴He bath. For efficient operation, the 0.3–20K temperature range was divided into three subintervals: 0.3–1.5K, 1.3–5.0K, and 4.2–20K. For temperatures greater than 4.2K, cooling was from ⁴He boiling under atmospheric pressure. Pumping the bath to low pressure with a large mechanical pump provided cooling to 1.2K and was necessary to condense the ³He, which was in turn pumped to near 0.25K by an oil diffusion pump.

C. Calorimeters

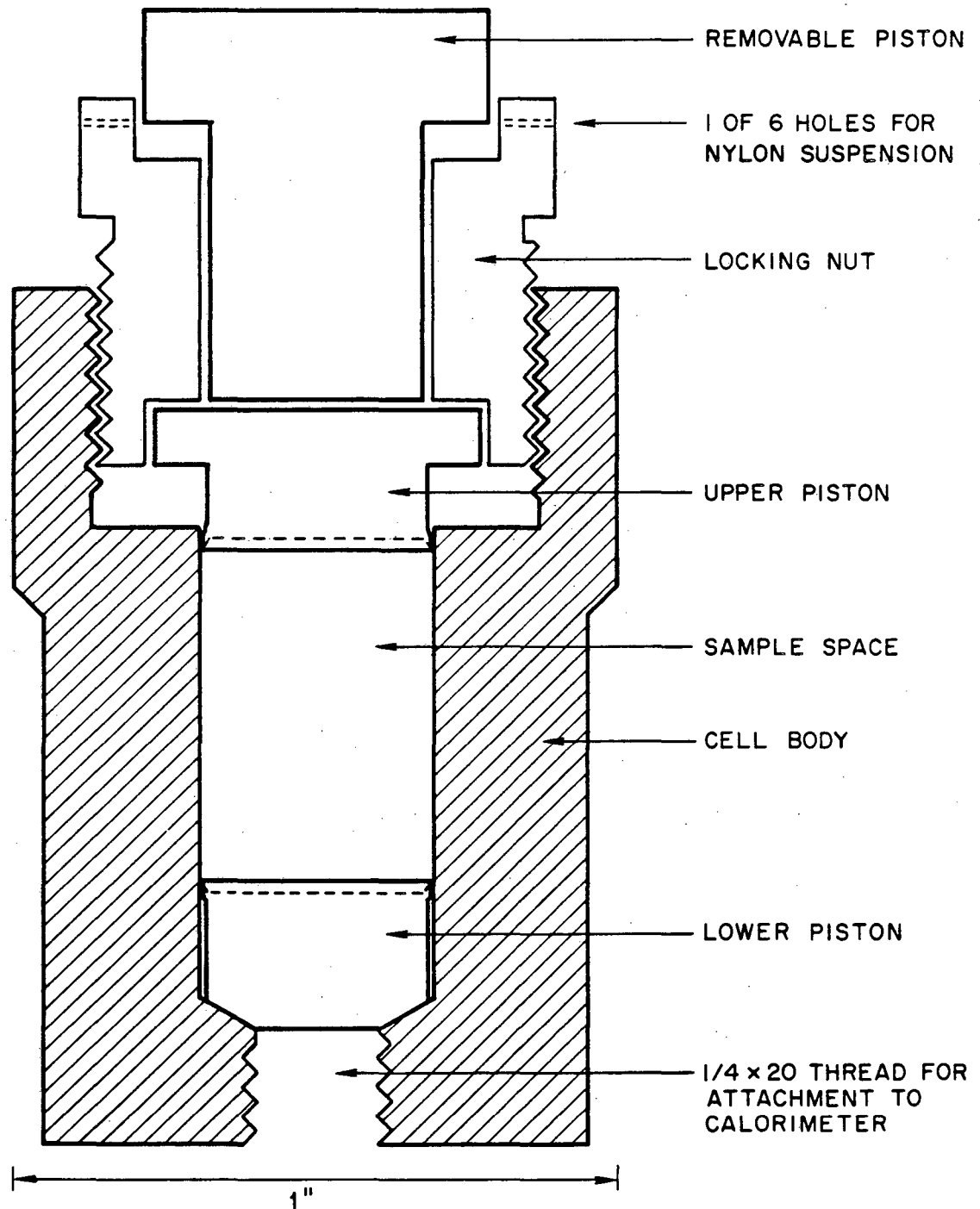
Two different calorimeters or sample holders were used in the cerium heat capacity measurements. The pressure dependence of the heat capacity of cerium was determined using a single calorimeter designed to contribute minimally to the addenda heat capacity. This calorimeter consists of a 6in. length of annealed 12 gauge OHFC copper wire to which is attached a germanium thermometer GE2347, a 10k Ω sample heater wound noninductively from 0.0009in. PtW resistance wire, a 1k Ω "background" heater wound noninductively from the same material, and a short 1/4–20 sample mounting screw machined from 99.9999 percent pure copper. The calorimeter is suspended from a brass cage, which is thermally anchored to the ³He pot, by nine nylon monofilament threads approximately one inch in length each. The thermometer body is attached with copper wire and epoxy and the thermometer leads are thermally anchored to the calorimeter with epoxy. Four 5in. lengths of 0.0009in. PtW wire provide electrical connection with thermal isolation for the thermometer. Three 4in. lengths of 0.003in. PtW wire are used for electrical connections of the sample heater, but

branch to four separate leads at the cage. The shared current and potential lead on one end of the heater automatically corrects for the heat dissipated in the heater current leads. Two 5in. lengths of 0.0009in. PtW wire make the electrical connection to the auxiliary heater used to compensate for temperature drifts.

The calorimeter used for heat capacity measurements in high magnetic fields was designed and built by Fogle.³³ There are three significant design differences in this calorimeter. The sample mounting screw was machined from high purity tungsten and a 99.9999 percent pure annealed silver wire is used to place the thermometer about 14in. from the sample and inside a mu-metal shield. With this arrangement, the dependence of the germanium thermometer calibration on applied magnetic field is negligible. The smaller nuclear moments of tungsten and silver in comparison to that of copper result in a magnetic field independent calorimeter heat capacity in fields up to 8T.

D. Pressure Cell

Figure 2 illustrates the pressure cell used in measuring the pressure dependence of the low temperature α -cerium heat capacity. The cerium contribution to the total measured heat capacity was maximized by making the sample volume of the cell as large as possible consistent with a 10kbar operating pressure range. The entire cell was constructed of beryllium-copper alloy to avoid large magnetic contributions to the cell heat capacity. The large cell bore diameter (0.375in.) results in large stresses on the pressure locking nut threads at the highest working pressure. In an earlier design using a



PRESSURE CELL

XBL 8112-12755

Fig. 2. Schematic drawing of the pressure cell used for high-pressure heat capacity measurements on α -Ce.

5/8-18 nut, the thread failed at 10kbar; however, a 3/4-20 nut with tighter machining tolerances proved adequate. Cerium undergoes compression of nearly twenty percent on application of 10kbar; moreover, it is impossible to completely fill the sample space when loading the cell at zero pressure. Consequently, a piston travel greater than 20 percent is necessary. A delta-ring like lip was machined onto both the upper and lower pistons to prevent extrusion of the sample at high pressure. This integral design provides for easier initial loading of the cell and reduces friction during compression.

E. Pressure Medium

Measurement of a physical property as a function of pressure requires reasonably uniform pressures. For many experiments, placing the sample in a self sealing teflon cup with a mixture of organic liquids produces good hydrostatic conditions.³⁵ In heat capacity measurements, however, any material in thermal contact with the sample or calorimeter contributes to the total measured heat capacity and must be accounted for quantitatively. Due to large dimensional changes occurring on taking cerium through the γ - α transition, it is difficult if not impossible to introduce and retain a quantitatively predetermined amount of liquid. The resulting uncertainty in the addenda heat capacity precludes the use of a liquid pressure transmitting medium. The use of a teflon cup without liquid was considered. Not surprisingly, teflon has a large and very pressure dependent heat capacity (see Part Three). Consequently, even small pressure inhomogeneities within the teflon cup result in an unpredictable pressure dependent contribution

to the addenda heat capacity. Solid silver chloride, which is the best insulating solid pressure transmitting medium known,³⁵ was tried in calibration runs at 0.5, 5.0, and 8.5kbar. The total measured heat capacities varied less than a 0.1 percent which corresponds to the expected combined resolution and reproducibility. Silver chloride also proved advantageous in that its relatively small thermal expansion coefficient leads to a close correspondence between the pressure applied at room temperature and that retained at low temperatures.

F. Pressure Measurement

The pressure applied at room temperature is not necessarily retained at low temperatures. In addition to changes arising from differential thermal expansion, incomplete transformation of γ to α cerium at room temperature leads to substantial loss of pressure as the transition is completed on cooling. These effects are beneficial in that pressures less than the room temperature transition pressure can be obtained at low temperatures. The pressure within the cell at low temperature is conveniently determined by use of a superconducting manometer.^{36,37} The pressure dependence of the superconducting transition temperature of tin is well known and provides a sensitive measure of pressure. The superconducting transition temperature of a small (0.35in. diameter x 0.005in.) tin disk, enclosed within the pressure cell, was detected with an ac mutual inductance bridge operated at 23Hz. A signal to noise ratio of about 50:1 was obtained and the transition temperatures were reproducible to within about 1mK which corresponds to 0.02kbar in pressure. The transition with an

unpressurized tin disk was about 20mK wide and was about 50mK wide in the highest pressure cerium experiment. The increase of 30mK in the transition width corresponds to a pressure inhomogeneity of 0.6kbar. In the series of experiments performed to determine the pressure dependence of the α -cerium heat capacity, changing the pressure from one experiment to the next resulted in a progressive broadening and the appearance of structure in the bridge response to the superconducting transition. On disassembling the cell, it was found that one edge of the tin disk had been pinched off and extruded into the space between the upper piston and cylinder wall. The structured bridge response evidently arose from the extruded tin going superconducting at higher temperatures or lower pressure. Assignment of the higher pressure transition to the tin within the sample chamber resulted in consistent behavior of the cerium heat capacity with pressure. Pressure inhomogeneity within the cell is estimated from the unstructured higher pressure transitions to be about 0.5kbar.

G. Samples

Two cerium samples, designated CE1 and CE2, from different material stocks, were produced at Ames Laboratory, Iowa State University for this heat capacity measurement. The samples were machined into 0.365in. diameter x 0.65in. cylinders, heat treated at 700K for four hours and electropolished. Subsequent handling was under an atmosphere of argon or dry nitrogen to avoid oxidation. Both samples had a nominal purity of 99.9 atomic percent. The maximum rare earth impurity concentration was 23.6 ppm for CE1 and 19.8 ppm for CE2. The maximum

magnetic transition metal impurity concentration was 4.5 ppm for CE1 and 8.5 ppm for CE2. Table I gives the detailed analysis of the two cerium samples. Seven heat capacity experiments at six different pressures were run on CE1. The heat capacity of CE2 was measured at a single pressure in several magnetic fields.

H. Pressurization

A silver chloride sheet³⁸ was rolled out to 0.005in. thickness and cut into three 0.375in. diameter disks and a 0.625 x 1.175in. rectangle. A single disk was placed into the cell bottom, the rectangular piece was carefully wrapped around the cerium sample, which was then inserted into the cell, and a 0.35in. dia. x 0.005in. disk of 69's tin was sandwiched between the remaining two silver chloride disk and placed into the top of the sample chamber. For the experiments on CE2, where the magnetic field dependence of the addendum heat capacity was measured with a fixed quantity of silver chloride (0.400g), the amount of silver chloride was adjusted to that quantity. The top piston, locking-nut, and removable piston were attached to the cell and the nut tightened. The cell was placed into a hydraulic press and the cerium compressed to the desired volume while observing the change in length of the cerium sample with a dial in-dicator gauge. At ambient temperature the γ - α transition is completed only above 7.5 kbar. To achieve appreciably lower pressures at low temperature, it is necessary to start with an allotropic mixture of γ - α cerium to obtain pressures below the room temperature transition pressure. As the partially transformed cerium is cooled more α -cerium is formed with an accompanying decrease in

Table I. Chemical Analysis of the Cerium Samples.

Impurity	CE1 Conc. (at. ppm)	CE2 Conc. (at. ppm)	Impurity	CE1 Conc. (at. ppm)	CE2 Conc. (at. ppm)
H	278.	278.	Rh	< 0.02	0.02
Li	0.02	< 0.02	Pd	< 0.06	< 0.05
Be	< 0.04	< 0.003	Ag	< 0.01	< 0.009
B	0.04	< 0.01	Cd	< 0.02	< 0.02
C	23.	47.	In	< 0.01	< 0.009
N	90.	100.	Sn	< 0.03	< 0.03
O	464.	385.	Sb	< 0.01	< 0.01
F	154.	192.	Te	< 0.02	< 0.02
Na	< 1.	0.04	I	< 0.01	< 0.01
Mg	< 0.02	< 0.01	Cs	< 0.001	< 0.001
Al	0.01	0.02	Ba	< 0.2	< 0.3
Si	1.	0.078	La	4.	9.
P	< 0.009	0.02	Pr	< 4.	< 1.
S	0.2	< 1.	Nd	8.	4.
Cl	4.	0.7	Sm	< 0.2	< 0.4
K	0.5	0.03	Eu	< 0.05	< 0.05
Ca	2.	0.2	Gd	< 10.	6.
Sc	0.14	0.3	Tb	< 0.6	< 1.
Ti	< 0.07	0.21	Dy	< 0.2	1.
V	< 0.008	0.014	Ho	< 0.07	< 1.
Cr	1.2	3.4	Er	< 0.3	5.
Mn	< 0.007	0.75	Tm	< 0.05	< 0.06
Fe	< 1.3	< 1.3	Yb	< 0.09	< 0.3
Co	< 0.01	0.004	Lu	< 0.1	0.9
Ni	2.	3.	Hf	< 0.3	< 0.3
Cu	1.4	2.	Ta	11.	6.
Zn	< 0.01	0.08	W	< 0.5	< 0.4
Ga	< 20.	< 0.2	Re	< 0.2	< 0.1
Ge	< 0.1	< 0.1	Os	< 0.2	< 0.2
As	< 0.01	0.02	Ir	< 0.1	< 0.08
Se	< 0.05	< 0.1	Pt	< 0.1	4.0
Br	< 0.01	< 0.1	Au	< 0.3	< 0.02
Rb	< 0.003	< 0.08	Hg	< 0.03	< 0.03
Sr	< 0.007	< 0.04	Tl	< 0.02	< 0.002
Y	1.4	< 10.	Pb	< 0.06	< 0.05
Zr	< 0.08	< 0.2	Bi	< 0.02	< 0.01
Nb	< 1.	< 20.	Ra	< 0.08	< 0.06
Mo	< 0.2	< 0.2	Th	< 0.2	< 0.2
Ru	< 0.1	< 0.09	U	< 0.09	0.3

sample volume leading to a loss in pressure. If the thermal expansions and compressibility of γ -cerium, α -cerium, silver chloride, and the beryllium copper cell were well known as a function of temperatures and pressure it would be possible to predict the final pressure accurately. But, lacking these data, it was empirically found that increasing the initial fraction of γ -cerium by a few percent of the total dropped the low temperature pressure several kbar. By this means final pressures as low as 2.3kbar were obtained.

J. Addenda Heat Capacity

The addenda heat capacities consist of contributions from the pressure cell, the silver chloride pressure transmitting medium, and the calorimeter, and contributes 80-90 percent of the total measured heat capacity depending upon temperature and pressure. Since the heat capacity of α -cerium is determined by subtraction of the addenda heat capacity from the total, the addenda heat capacity must be characterized and reproducible to within about 0.1 percent to obtain the cerium heat capacity accurate to better than 1 percent. The heat capacity of the calorimeter and pressure cell without silver chloride was measured in two separate experiments and found to be reproducible to better than 0.1 percent. The cell was loaded with 0.506g silver chloride and 9.035g of 99.9999 percent pure copper from a stock previously measured. The heat capacity was measured at 0.5, 5.0 and 8.0 kbar and found to agree to within 0.1 percent. Subtraction of the calorimeter, pressure cell, and pure copper heat capacities yielded the heat capacity of silver chloride. The silver chloride heat capacity ranged from

0.2–3.0 percent of the total and was in agreement with the 2–20K measurement reported by Berg.³⁹ Below 2K the heat capacity of the silver chloride diverged from the expected cubic temperature dependence. The divergence was probably due to contributions from impurities in the silver chloride. An eight term polynomial was used to represent the silver chloride heat capacity to within 3 percent for temperatures 0.3–20K. The error introduced by uncertainties in the silver chloride heat capacity is negligible at temperatures less than 4K and less than 0.1 percent at higher temperatures.

For the addenda calibration in magnetic fields, a somewhat different procedure was followed in that a fixed quantity of silver chloride (0.400g) was chosen for all runs. The heat capacity of the pressure cell, 0.400g AgCl, 9.064g of copper, and the high field calorimeter was measured in five magnetic fields (0.0, 1.5, 3.0, 5.0, and 7.5T) for the temperature interval 1.3–5K. Measurements at lower temperatures were omitted due to an expected large field dependence from the beryllium copper hyperfine and magnetic impurity contributions to the addenda heat capacity. The observed addendum heat capacity varied by up to 15 percent as the magnetic field shifted impurity contributions to higher temperatures. Overall precision and reproducibility was again about 0.1 percent.

III. RESULTS AND ANALYSIS

A. Heat Capacity Experiments

The heat capacities of two samples of α -cerium from different material stocks were determined as a function of pressure and magnetic field. Table II gives the details of the experiments with respect to sample, temperature range, pressure, and magnetic field. The pressure dependence of the heat capacity was determined from seven experiments at six pressures, ranging from 2.3 to 9.0kbar, on the sample designated CE1. Experimental runs 2 and 3 were at essentially the same pressure. The pressure was released and reapplied between these two runs to check reproducibility of the heat capacity with pressure. In the lowest pressure run (2.3kbar), heat capacity data indicated that about 0.3 percent of the β -cerium allotrope was present. At higher pressures, however, the samples were without β -cerium. These runs were made in the order of decreasing pressure except that in the final experiment the pressure was increased to 4.3 kbar as a check for progressive sample oxidation or the introduction of mechanical defects.

The second sample, CE2, was loaded and compressed to a volume that gave a low temperature pressure of 5.2kbar. Its heat capacity was measured using the same experimental setup as in the experiments on CE1 for a check of sample dependent effects. The pressure cell and sample were then transferred, without changing the pressure, to a different apparatus designed for heat capacity measurements in high magnetic fields, but in which there was no provision for monitoring the superconducting transition of the tin manometer. The heat capacity

Table II. Details of Externally Controlled Parameters.

Run	Sample	P (kbar)	H (T)	T (K)
1	CE1	9.0	0.00	0.3-20
2	CE1	7.4	0.00	0.3-20
3	CE1	7.4	0.00	0.3-20
4	CE1	6.8	0.00	0.3-20
5	CE1	5.4	0.00	0.3-20
6	CE1	2.3	0.00	0.3-20
7	CE1	4.3	0.00	0.3-20
8	CE2	5.2	0.00	0.3-20
9	CE2	5.2	0.00	1.3-4
10	CE2	5.2	1.50	1.3-4
11	CE2	5.2	3.00	1.3-2.6
12	CE2	5.2	5.00	1.3-3.0
13	CE2	5.2	7.50	1.3-4

was measured over a restricted temperature range in five magnetic fields ranging from 0 to 7.5T.

B. Data Analysis Technique

The heat capacity of α -cerium at each pressure and magnetic field was evaluated as $C(T,P,H) = C_{\text{tot}}(T,P,H) - C_{\text{add}}(T,H)$, where $C_{\text{tot}}(T,P,H)$ is the total measured heat capacity at temperature T , pressure P , and applied magnetic field H and $C_{\text{add}}(T;H)$ is the pressure independent but highly field dependent addenda heat capacity. The heat capacity of the cerium sample in these experiments ranged from 10 to 20 percent of the total measured heat capacity depending upon the exact temperature, pressure, and magnetic field. The resulting cerium heat capacities have a precision of about 0.5 percent and an estimated overall accuracy of about 1 percent. In theory, the specific heat of α -cerium has no magnetic, crystal field, or nuclear hyperfine contributions, and should be simply the sum of the electronic and lattice specific heats. At low temperatures, the electronic specific heat depends linearly on the temperature and is expressible as $C_E = \gamma T$, where $\gamma = \pi^2 k_B^2 N(E_F)(1+\lambda)/3$. The factor $N(E_F)$ is the bare electronic density of states at the Fermi level and λ lumps together the electron effective mass enhancements from the electron-phonon and electron-electron interactions. For sufficiently low temperatures, only those lattice vibrational modes for which dispersion is negligible are excited; consequently, the Debye model is valid, and the lattice specific heat has a cubic temperature dependence expressible as $C_L = A_3 T^3$, where $A_3 = 12/5 \pi^4 R \theta_0^{-3}$, and θ_0 is the low temperature Debye characteristic

temperature. At higher temperatures the lattice specific heat includes higher odd powers of T , $A_5 T^5$ etc. The linear approximation to the electronic specific heat may not be entirely appropriate for α -cerium which exhibits intermediate valence behavior. The non-interacting fermi-liquid theory of the intermediate valence state of Newns and Hewson,⁴⁰ however, predicts a negligible T^3 contribution from the electronic system for $T < 10K$. It has also been suggested that there may be an appreciable spin-fluctuation contribution to the specific heat of α -cerium.²¹ In addition to an enhancement to the linear electronic specific heat, theory predicts a $T^3 \ln T$ contribution. There is, however, no reliable estimate of the importance of the $T^3 \ln T$ component which might be obscured by the lattice contribution. For the purpose of further analysis and discussion it will be assumed that the linear contribution to the heat capacity is of electronic origin and that higher order contributions are due to the crystal lattice.

The low temperature heat capacity of α -cerium is therefore simply the sum of the electronic and lattice specific heat. It then follows, since $C/T = \gamma + A_3 T^2$, that C/T when plotted versus the T^2 should fall on a straight line with intercept γ and slope A_3 . Figure 3, which displays the low temperature heat capacity data for CE1, shows that C/T is linear only over a narrow range of temperatures. For temperatures less than 1.2K, two low temperature anomalies are significant and for temperatures greater than 2.2K, deviations from the low temperature limiting T^3 behavior of the Debye model become important. The

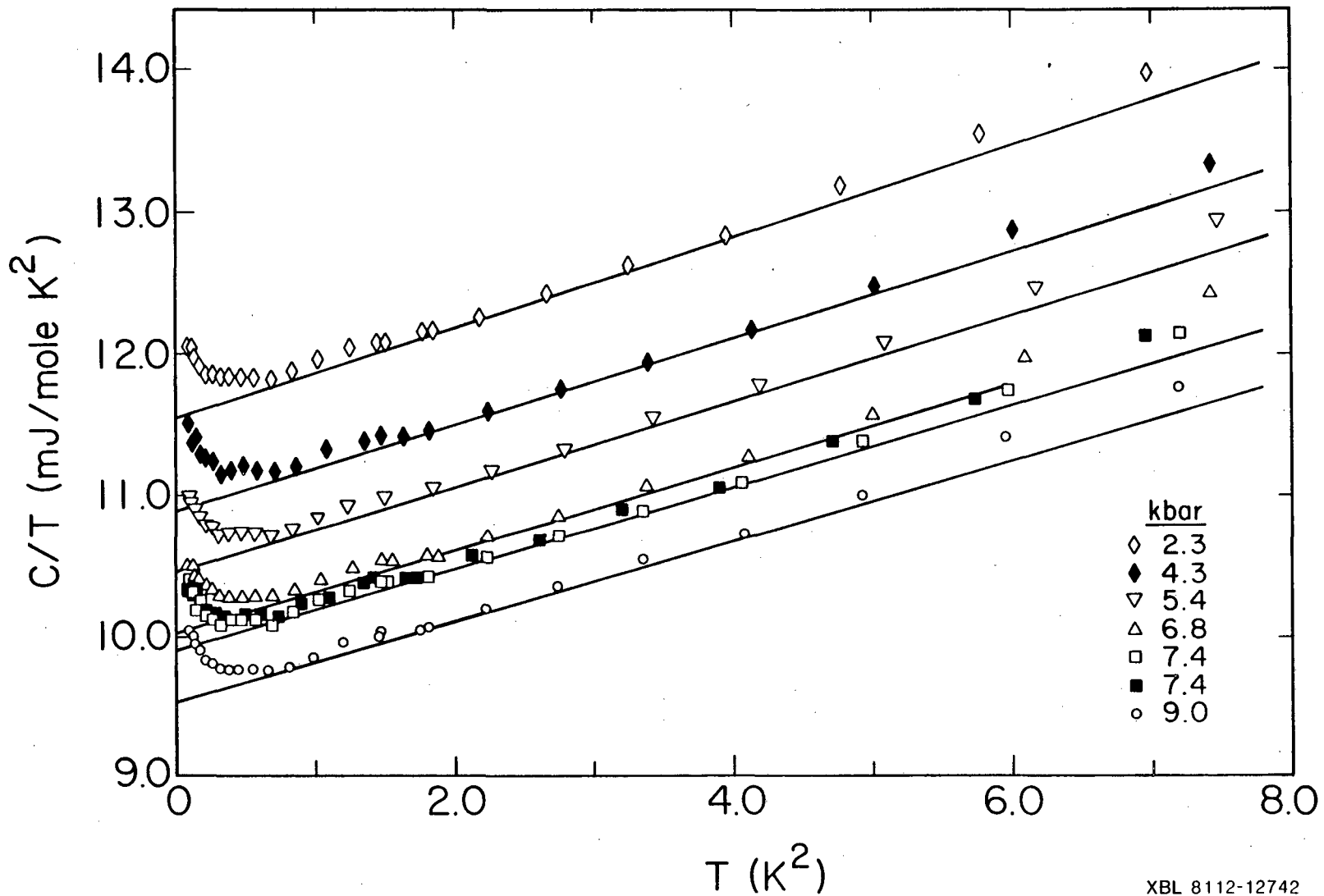


Fig. 3. The low-temperature heat capacity data for CE1 at several pressures.

narrow temperature range over which C/T is linear in T^2 limits the accuracy with which the electronic and lattice specific heats can be separated by either straightforward graphical or least-square techniques. Figure 4 shows the relative electronic and lattice specific heats at one pressure (6.8kbar) from which it is seen that the electronic specific heat is more than 90 percent of the total for temperatures less than 2K and that the lattice specific heat is dominant only at temperatures well above that at which the T^3 approximation is accurate. The dominance of the electronic specific heat at the lowest temperatures permits an initial estimate of γ from the C/T versus T^2 plot. Subtraction of this estimated electronic specific heat from the total and division by T^3 yields $(C-\gamma T)/T^3 = A_3 + \delta\gamma/T^2 + A_5T^2 + O(T^4)$, where $\delta\gamma$ represents the error in estimating γ and $O(T^4)$ denotes higher order lattice contributions. The term $\delta\gamma$ shows up as a divergence at low temperatures in plots of $(C-\gamma T)/T^3$ if $\delta\gamma$ is not small. By adjusting γ such that $(C-\gamma T)/T^3$ falls on a straight line at low temperatures when plotted versus T^2 , γ 's are obtained with a precision of a few tenths of a percent and the intercepts are the T^3 coefficient of the lattice heat capacity ($A_3 = 12/5 \pi^4 R \theta_0^{-3}$). Figure 5 shows plots of $(C-\gamma T)/T^3$ versus T^2 for the seven experiments on CE1. The slopes of these curves are the T^5 lattice heat capacity coefficients and the positive curvature, produced by still higher order terms, further emphasizes the relatively low temperatures at which dispersion effects become important. Figure 6 displays the low temperature heat capacity data from the experiment on CE2 at 5.2kbar. The absence of anomalous

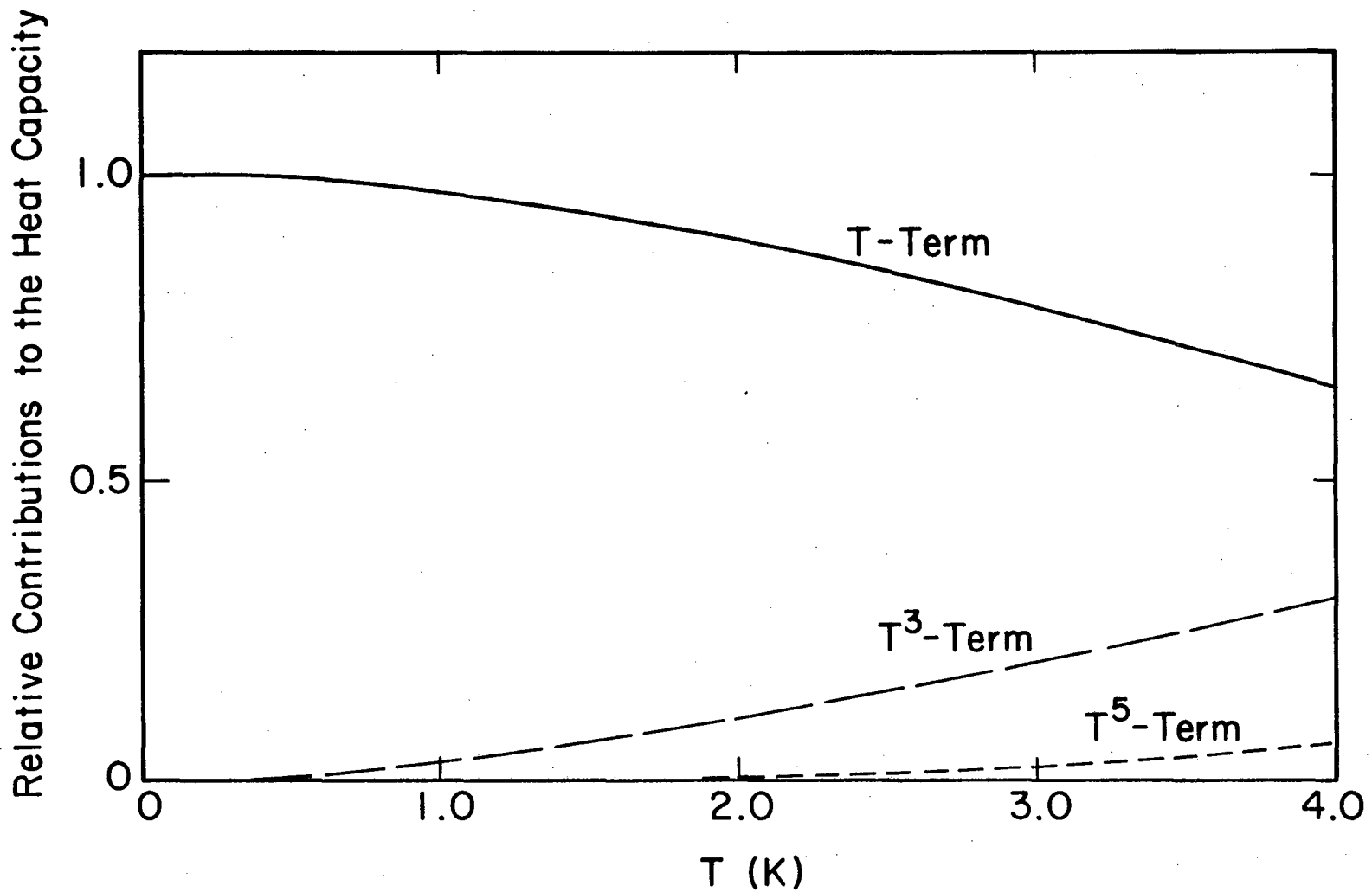
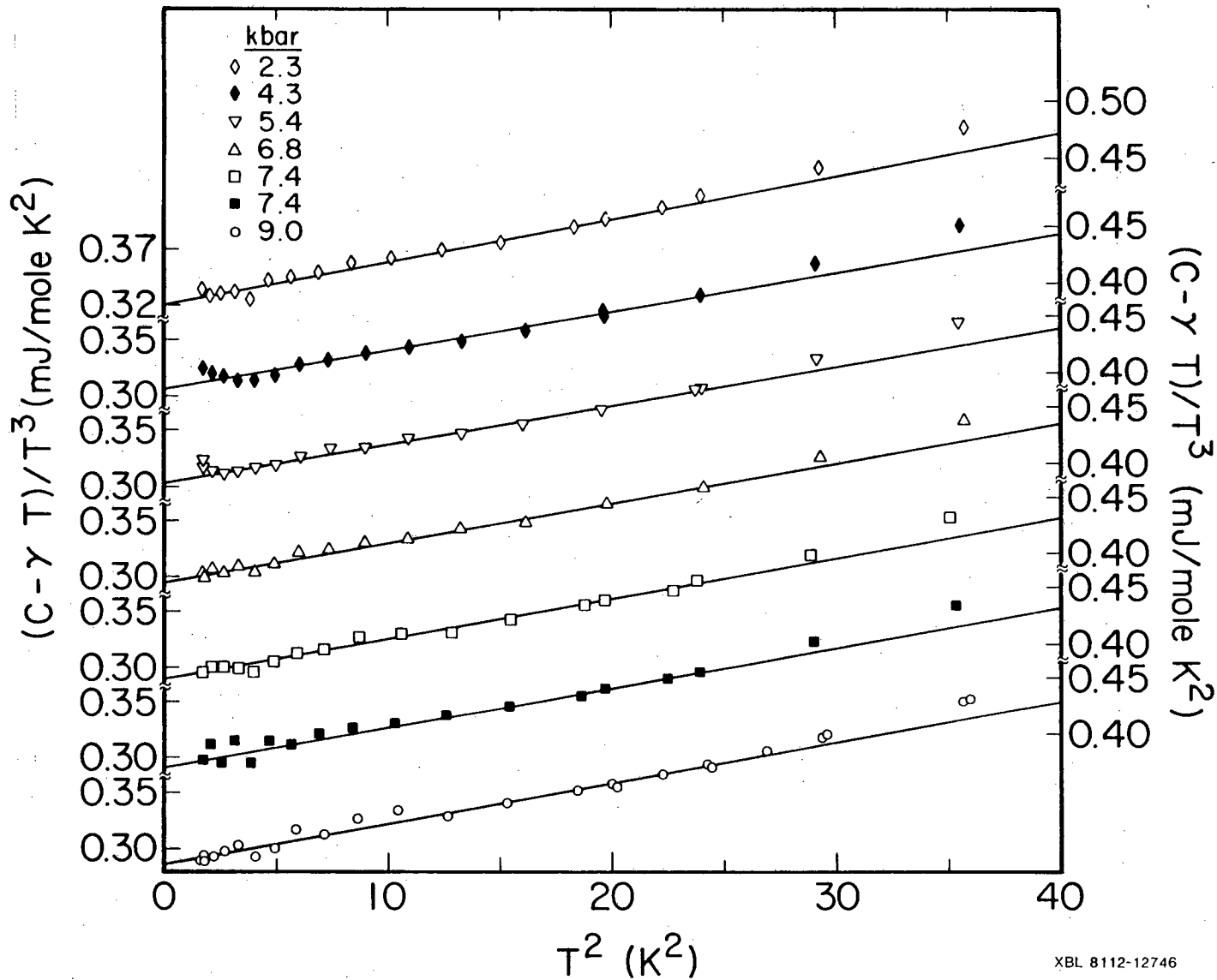


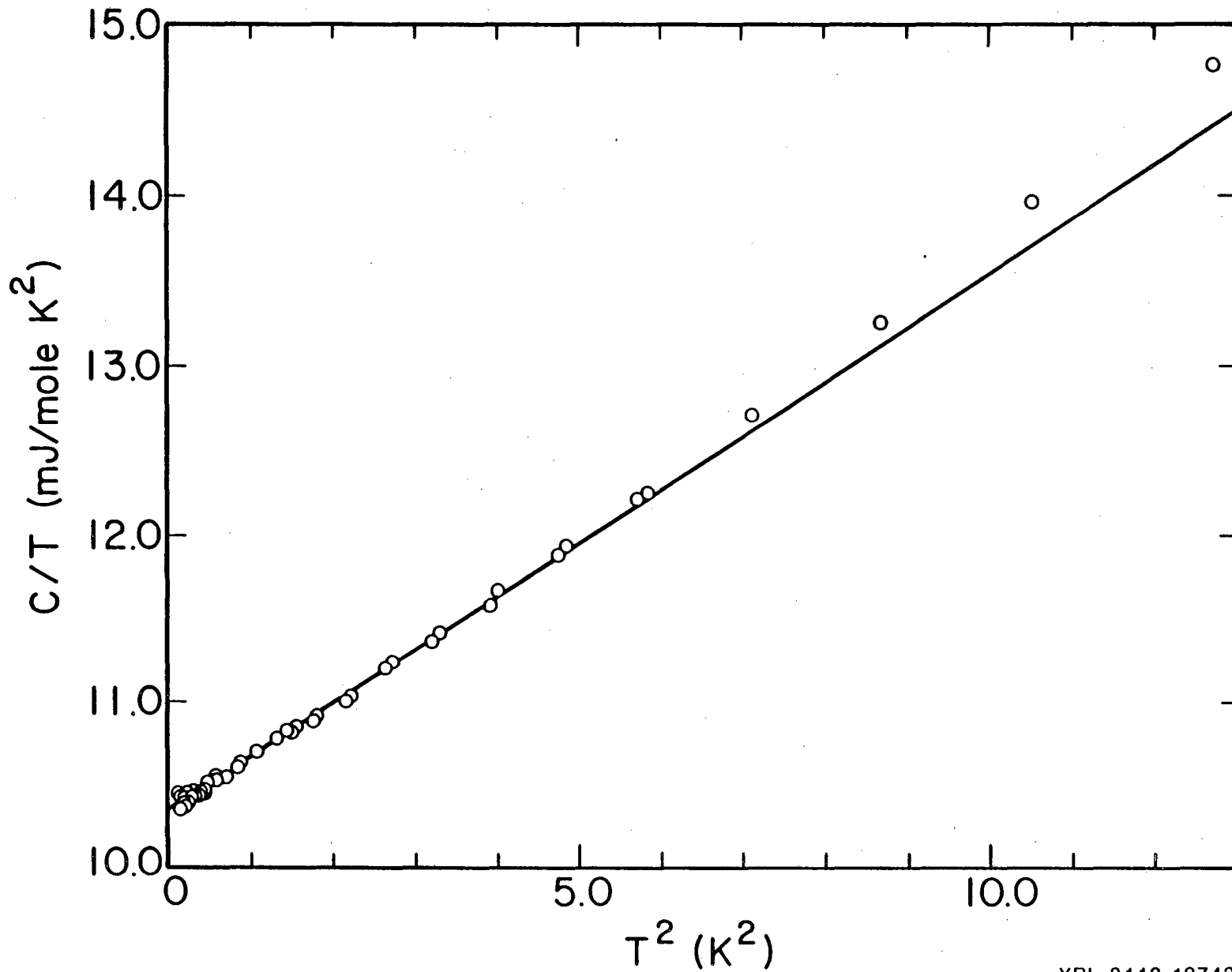
Fig. 4. The fractional contributions of the electrons and the lattice to the heat capacity of α -Ce at 6.8kbar.

XBL 8112-12754



XBL 8112-12746

Fig. 5. The low-temperature lattice contribution to the lattice heat capacity of α -Ce at several pressures. The slope of these curves represents the T^5 term.



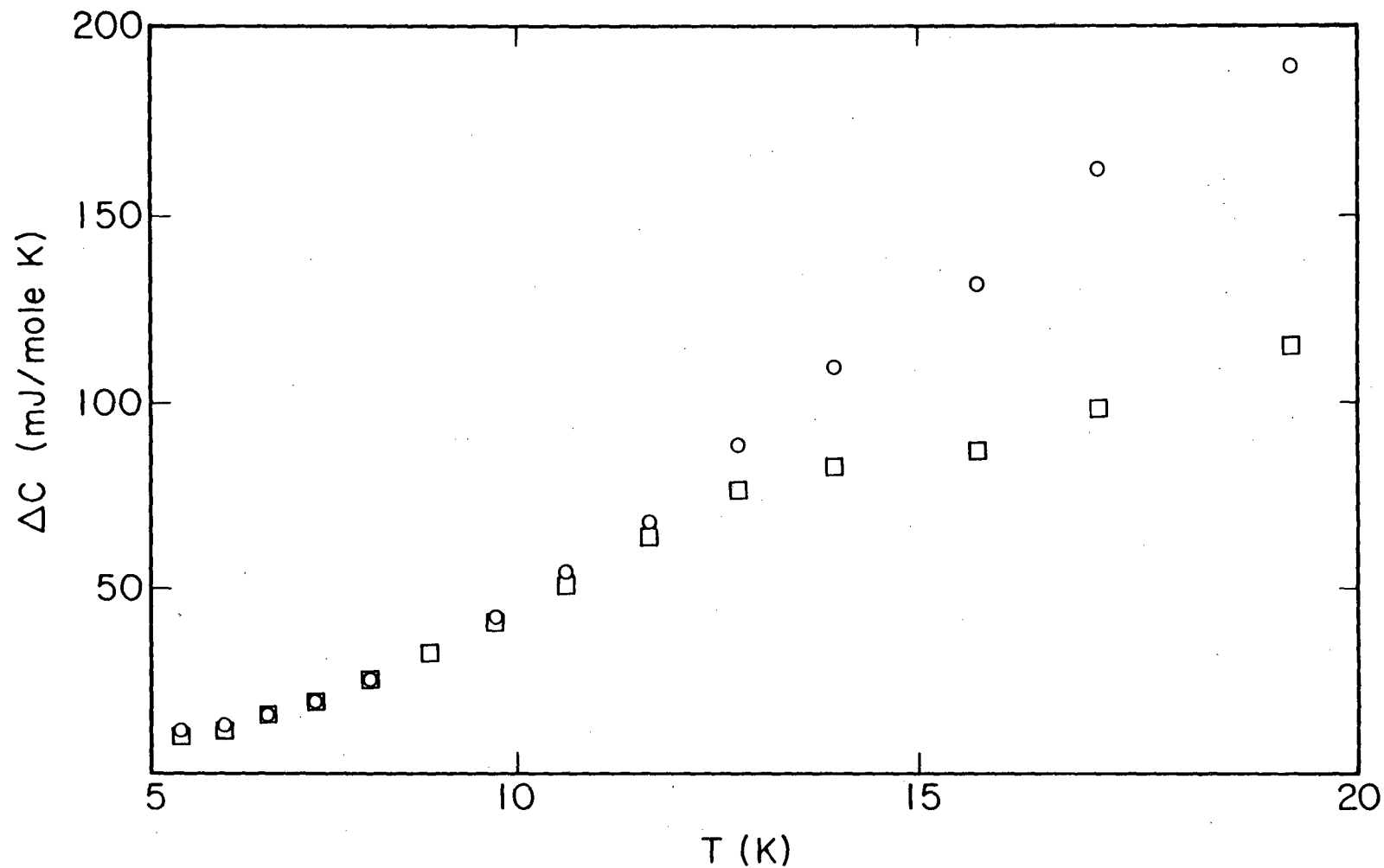
XBL 8112-12743

Fig. 6. The low-temperature heat capacity data of sample CE2 at 5.2 kbar.

low temperature contributions in the heat capacity of this sample permits straightforward extraction of γ and θ_0 from the intercept and slope of a C/T versus T^2 plot of the data. The values obtained are identical to those obtained using the method described in analysis of the CE1 data. While the θ_0 obtained for CE2 is in excellent agreement with those of CE1, γ is nearly one percent lower than expected from interpolation of the CE1 data and indicates that the effects of the sample dependent anomalous contributions in the heat capacity of CE1 may not have been entirely eliminated.

C. β -cerium Contributions

The presence of β -cerium can have an important effect on experimental heat capacities of α -cerium due to the large magnitude of the heat capacity associated with antiferromagnetic ordering near 12.5K.²⁷ The heat capacity data from individual experiments showed no direct evidence of a peak associated with antiferromagnetic ordering of β -cerium. However, as shown in Figure 7, the difference $C(T)_{p=2.3} - C(T)_{p=4.3}$ plotted as a function of T showed a bump at 12.5K with the magnitude of the bump corresponding to approximately 0.3 percent β -cerium, although the difference $C(T)_{p=4.3} - C(T)_{p=9.0}$ showed no structure near 12.5K. This was taken as evidence that β -cerium was present in detectable amounts only in the 2.3kbar run and that there was 0.3 percent β -cerium present in that run. The data for that run were corrected for the estimated β -cerium contribution, i.e., to $(C - 0.003C_\beta)/0.997$ where C_β is the heat capacity of β -cerium from the experiment of Koskenmaki and Gschneider.⁴¹ The values of γ and



XBL 823-8359

Fig. 7. The differences, $\Delta C = C(T)_{p=2.3} - C(T)_{p=4.3}$ (\square) and $\Delta C = C(T)_{p=4.3} - C(T)_{p=9.0}$ (\circ), plotted as a function of T . The symbols represent differences between actual data points that were taken at essentially the same temperature.

ϵ_0 obtained after this correction were entirely consistent with both previous zero pressure work and the present high pressure results. Figure 8 displays the lattice specific heat in the temperature region of the β -cerium antiferromagnetic ordering peak and shows the absence of any β -cerium derived structure.

D. Anomalous Low-Temperature Contributions

The heat capacity of sample CE1 has two low temperature anomalies which, from comparison with the heat capacity of sample CE2, are obviously sample dependent contributions. In Figure 9, the pressure dependent sum of the electronic and lattice heat capacities has been subtracted from the measured heat capacity of each pressure and the remainder plotted versus temperature. The remainder clearly shows the presence of two pressure independent contributions. The largest increases with decreasing temperature and is about 5 percent at 0.3K and the smaller is a bump of about 1 percent with a maximum near 1.2K. The small apparent variation of these data with pressure is insignificant within the precision of the data and the accuracy with which the electronic and lattice specific heats are determined. The resolution of these two features is insufficient to accurately characterize their temperature dependence. The largest anomaly falls as approximately T^{-1} rather than T^{-2} as would be expected for the high temperature limit of a Schottky peak and the smaller anomaly at higher temperatures appears too sharp for a Schottky anomaly. Comparison of the impurity concentrations present in the two samples shows no obvious culprit for either anomaly. It is also unlikely that

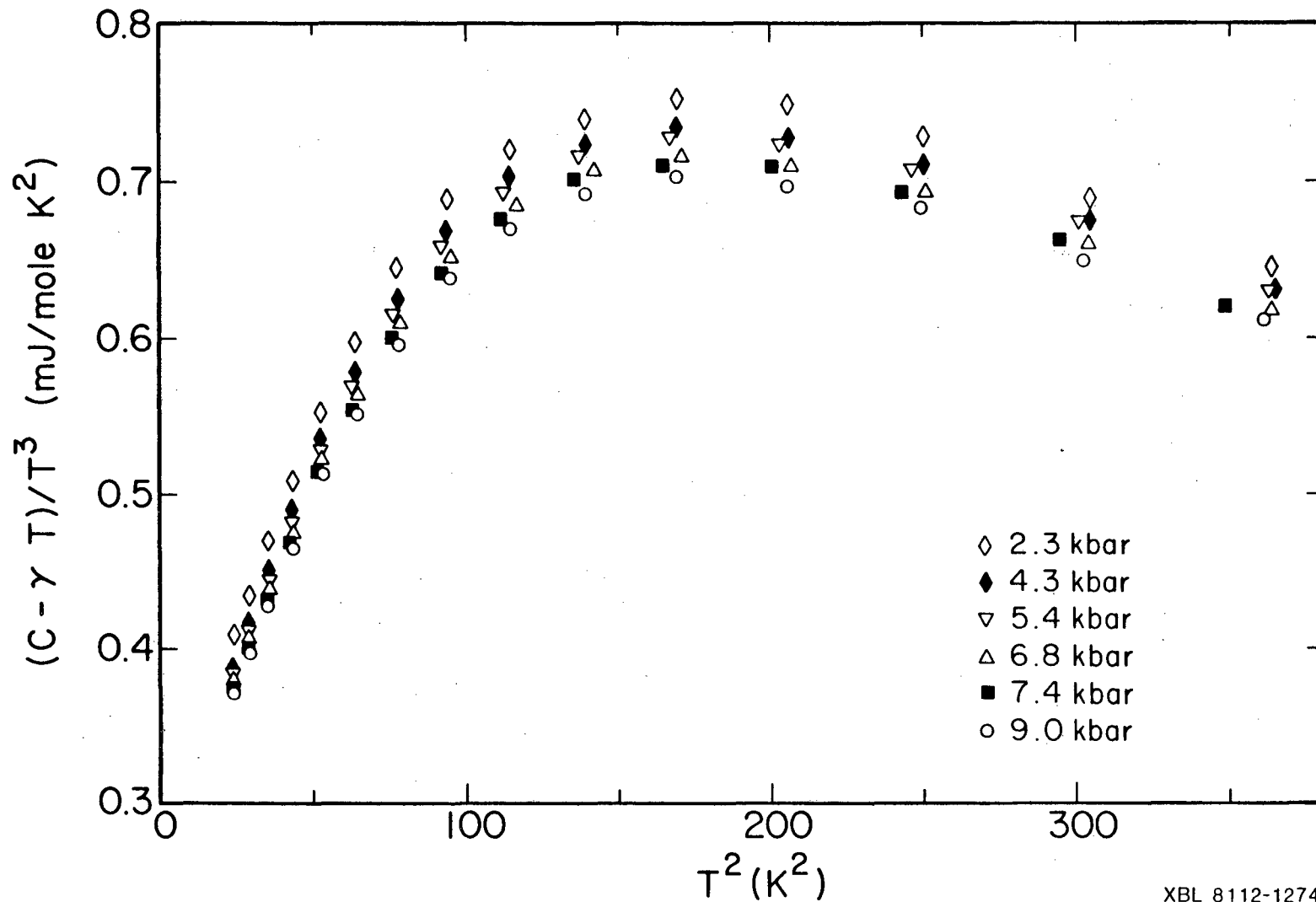


Fig. 8. The lattice heat capacity of CE2 at several pressures. The smoothness of the data near 12.5K ($T^2 \approx 160K^2$) shows that the β -phase makes no important contribution.

XBL 8112-12740

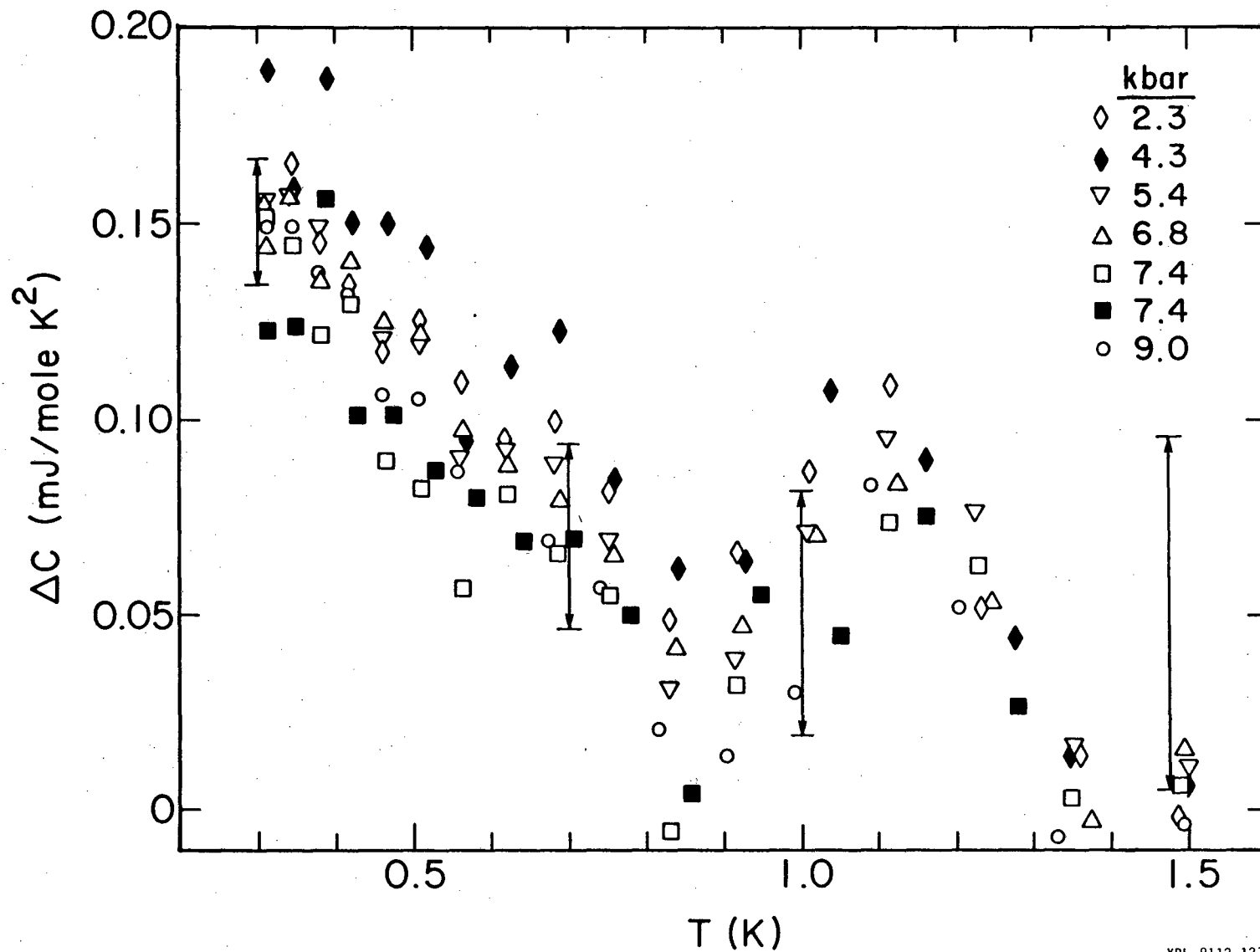


Fig. 9. The anomalous low-temperature contributions to the heat capacity of CE₂ ($\Delta C = C(P_i, T) - [Y_i T + A_3 i T^3 + A_5 i T^5]$). The vertical bars represent 0.1% of the total measured heat capacity.

XBL 8112-12756

surface oxidation of CE1 is at fault as Conway measured the heat capacity of a cerium sample before and after heavy oxidation and observed no significant differences in the temperature region of interest.²¹ Gschneidner and Thome have proposed hydrogen tunneling as an explanation of a low temperature tail in the heat capacity of lutetium.⁴⁰ While the quantities of hydrogen and other dissolved gases in CE1 are consistent with a similar interpretation, the absence of this feature in the heat capacity of CE2, which has comparable quantities of these dissolved gases, reduces the likelihood of this explanation. The bump at 1.2K is similar to peaks observed by Conway at 0.9K for several samples,²⁴ but is a factor of forty smaller in the present experiment. The rare earth and transition metal impurity concentrations in the samples measured by Conway were typically two orders of magnitude larger than those of the present sample, which supports the interpretation that this peak is an impurity contribution. It is also unlikely that the presence of β -cerium accounts for either of the anomalies as the concentration of β -cerium present would be a strong function of pressure and thermal history. While the exact origin of the two anomalies present in the heat capacity of CE1 is uncertain, the sample dependence points out impurity contributions as the most likely origin.

E. Pressure Dependence

The values of the electronic specific heat coefficient, γ , and the low-temperature Debye characteristic temperature, θ_0 , determined as a function of volume (pressure) from experiments on samples CE1

and CE2 are presented in Table III. The low-temperature heat capacity data at zero pressure from the experiment of Koskenmaki and Gschneidner²⁷ were reanalyzed by the graphical technique described earlier. This technique results in a better separation of the electronic and lattice contributions to the heat capacity of α -cerium than least-square analysis which is more sensitive to the temperature range of the data included in the fit, the polynomial form to which the data are fit, irregularities in the temperature scale, and precision of the data. Reanalysis results in a γ of 12.4 mJ/mole-K² as opposed to 12.8 mJ/mole-K² originally reported and a θ_0 of 179K unchanged from the earlier analysis. Figure 10 displays the volume dependence of γ and θ_0 and show that the data are well represented by a linear function of $\ln(V/V_0)$ where V_0 is the volume of α -cerium at zero pressure. A least-square analysis of the data gave $\gamma(V) = 12.34 [1 + 10.38 \ln(V/V_0)]$ mJ/mole-K² with a RMS deviation of 0.5 percent and a maximum deviation of less than 1 percent. The least-square result for θ_0 is $\theta_0(V) = 179 [1 - 2.58 \ln(V/V_0)]$ K with a RMS deviation of 0.1 percent and maximum deviation of 0.2 percent. The major source of the deviations from these two relations comes from uncertainty in the pressure or volume assigned to each experiment. A least-square fit of $\ln \theta_0$ to $\ln(V/V_0)$ produced a value of the Gruneisen constant = $-d \ln \theta_0 / d \ln V$ of 2.51. The data are equally well fit by either of these relations. Comparison of the present work with the previous high pressure heat capacity results of Phillips, Ho, and Smith at an estimated pressure of 11kbar show a large discrepancy.

Table III. Results of the Low Temperature Analysis of the Heat Capacity Data.

Run	p (kbar)	$\ln [V/V_0]^a$	γ (mJ/mole-K ²)	θ_0 (K)
KG ^b	0	0	12.4	179.0
CE1-6	2.3	-0.0063	11.50	182.3
CE1-7	4.3	-0.0116	10.88	185.0
CE2-1	5.2	-0.138	10.35	185.6
CE1-5	5.4	-0.0141	10.46	185.8
CE1-4	6.8	-0.0177	10.02	187.4
CE1-3	7.4	-0.0191	9.88	188.5
CE1-2	7.4	-0.0191	9.90	188.3
CE1-1	9.0	-0.0227	9.50	189.4

a Atomic volumes were obtained from pressure through the data of Francischi and Olcese²⁸ corrected for thermal expansion to 0K.

b From reanalysis of the data of Koskimaki and Gschneidner²⁷ consistent with analysis used in the present work.

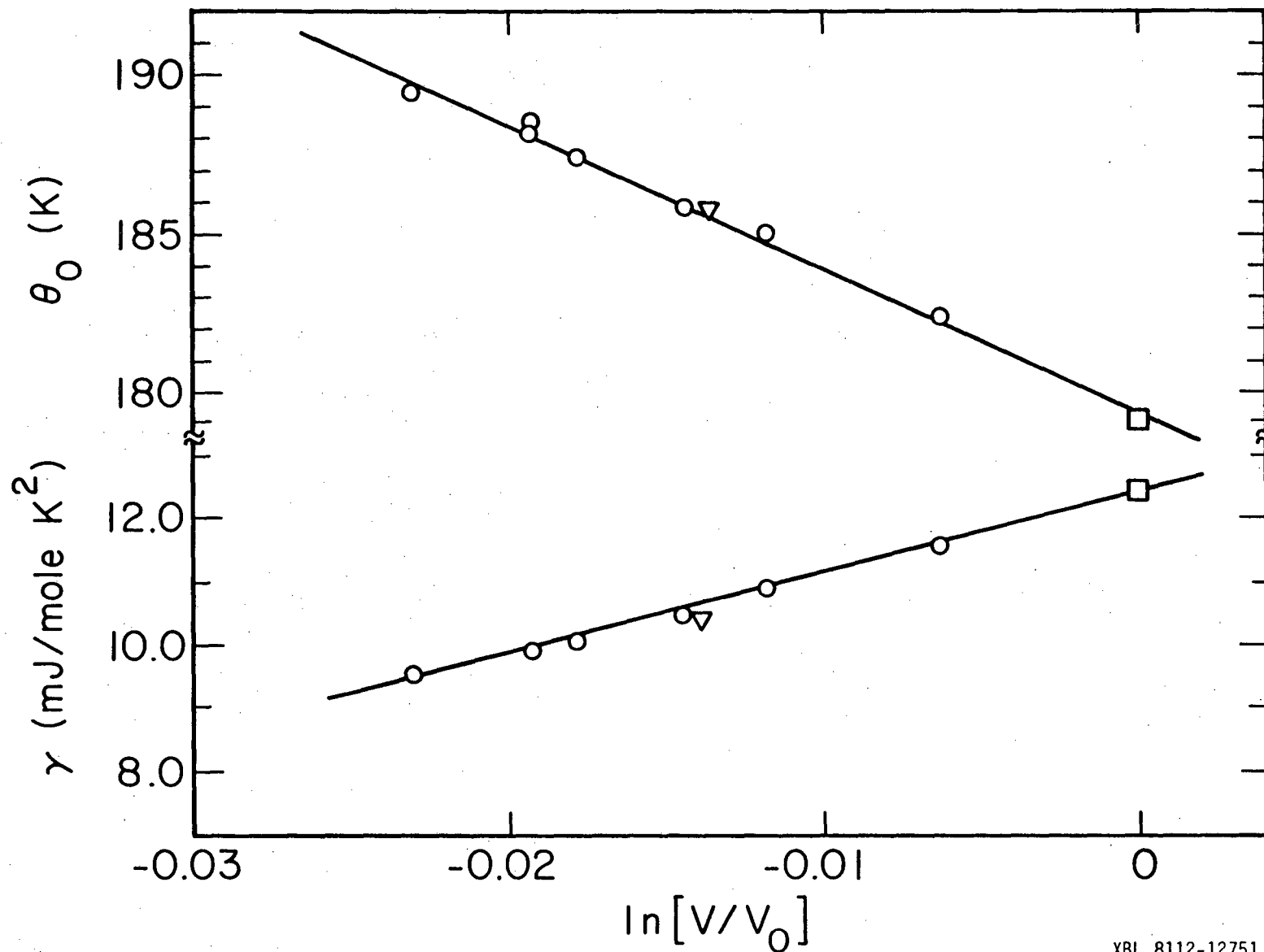


Fig. 10. The volume dependence of γ and θ_0 . The squares are from Ref. 27 (see text), the circles from the CE1 data, and the triangles from the CE2 data.

XBL 8112-12751

These new results imply a γ at 11kbar of 8.8 mJ/mole-K² as opposed to their reported γ of 11.3 mJ/mole-K² and a θ_0 of 192K as opposed to their 200K. The origin of this discrepancy is most probably a combination of several factors. First, the pressure of 11kbar was estimated rather than measured in situ. Secondly, the purity of their sample was much poorer than that used in the present experiment. Finally, their cerium sample contributed only about 2 percent of the total measured heat capacity, consequently the data are characterized by substantial experimental uncertainty. Figure 11 compares the 11kbar data with an extrapolation of the present work represented as $C = \gamma T + A_3 T^3 + A_5 T^5$. A substantial upturn in C at the lowest temperatures has clearly led to an overestimate of γ and θ_0 for the 11kbar experiment.

F. Thermal Expansion Coefficient

The relatively strong pressure dependence of the heat capacity of α -cerium permits evaluation of the thermal expansion coefficient, $\beta = 1/V (\partial V/\partial T)_P$, from the pressure derivative of the third law entropy through the thermodynamic relation $(\partial S/\partial P)_T = (\partial V/\partial T)_P = -V\beta$. Measurement of the zero pressure thermal expansion of α -cerium by conventional techniques would be a formidable experiment requiring a difficult pressure temperature cooling cycle similar to that first described by Panousis and Gschneidner.²³ The only previous low temperature thermal expansion measurement on cerium was on an allotropic mixture of α and β -cerium.⁴³ In that experiment β -cerium was the dominant constituent. The third law entropy was obtained as a function of temperature and pressure through integration of $C_p(T,P)/T$.

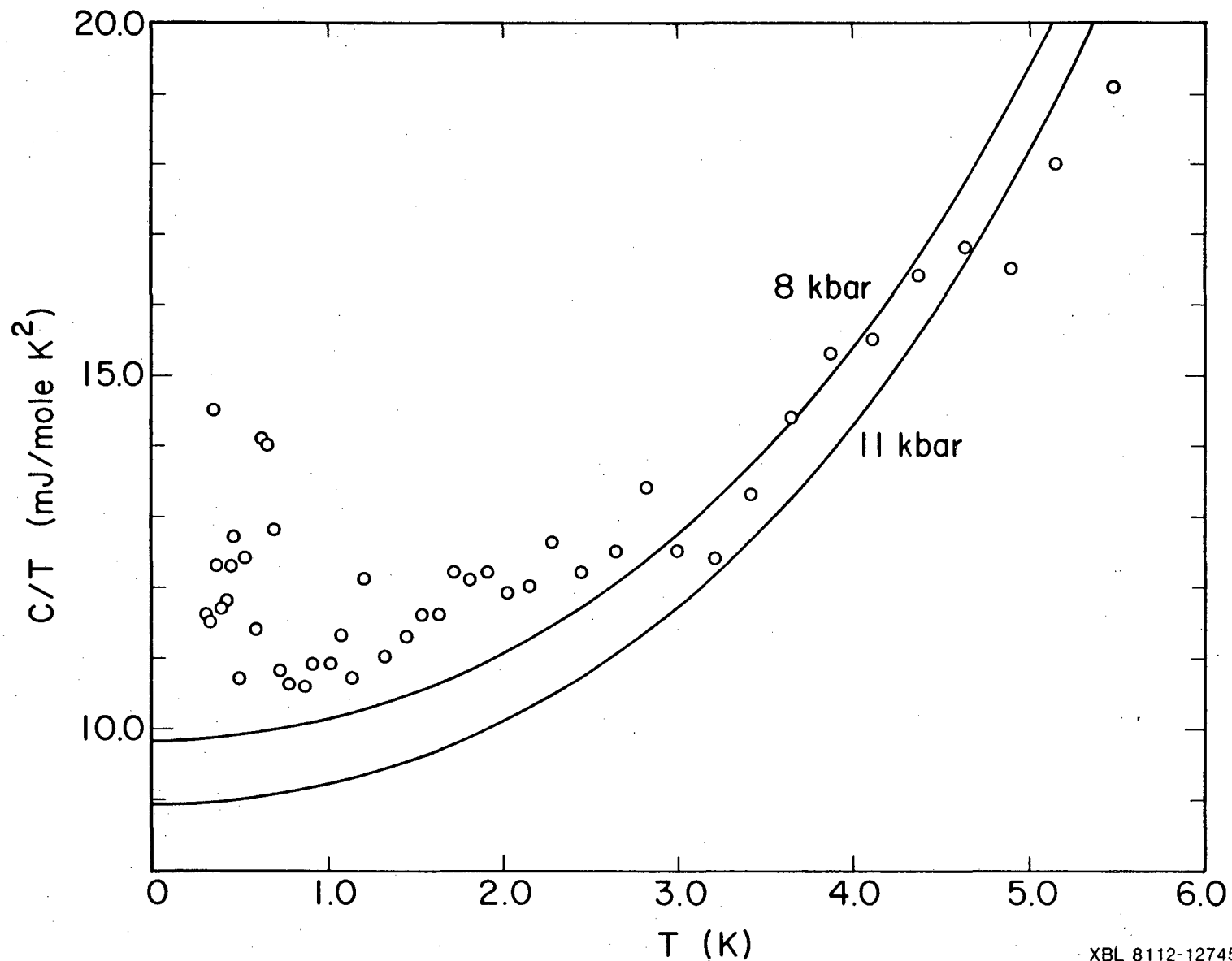


Fig. 11. A comparison of the α -cerium heat capacity data of Ref. 26 with estimates for 8 and 11kbar from the present work. XBL 8112-12745

A double smoothing operation was employed in computation of β and a different procedure used for temperatures below and above 2K. In the low temperature limit ($T < 2K$)

$$\beta = -V^{-1} \left(\frac{\partial S}{\partial P} \right)_T = (VB_T)^{-1} \left[\frac{d\gamma}{d \ln V} T - \frac{12}{5} \pi^4 R \left(\frac{T}{\theta} \right)^3 \frac{d \ln \theta_0}{d \ln V} \right]$$

where B_T is the isothermal bulk modulus. The quantities $d\gamma/d \ln V$ and $d \ln \theta_0 / d \ln V$ have uncertainties of a few percent with the largest uncertainty associated with assignment of pressure or volume to the measured heat capacities. For $T > 2K$, the lattice contribution to the entropy has higher order terms and the entropy was obtained by numerical integration of smooth curves drawn through the heat capacity data and addition of the direct integral of $C_p = \gamma(P) T + A_3(p) T^3$ from 0.0 to 2.0K. For selected temperatures the entropy was least square fit to $S(V)_T = S(V_0)_T + (dS/d \ln V)_T \ln(V/V_0)$ and the thermal expansion coefficient obtained as $\beta = (VB_T)^{-1} (dS/d \ln V)_T$. At 2K, where β was computed by both methods, agreement is within 0.2 percent. The results are displayed in Figure 12 and numerical values are given in Table IV. Determination of the low temperature thermal expansion coefficient β allows us to estimate the difference $C_p - C_v$, which can be important in some materials even at low temperatures. From $C_p - C_v = TV\beta^2 B_T$, where V is the cerium molar volume and B_T is the isothermal bulk modulus, and using the thermal expansion data derived from the pressure dependence of the heat capacity, the difference

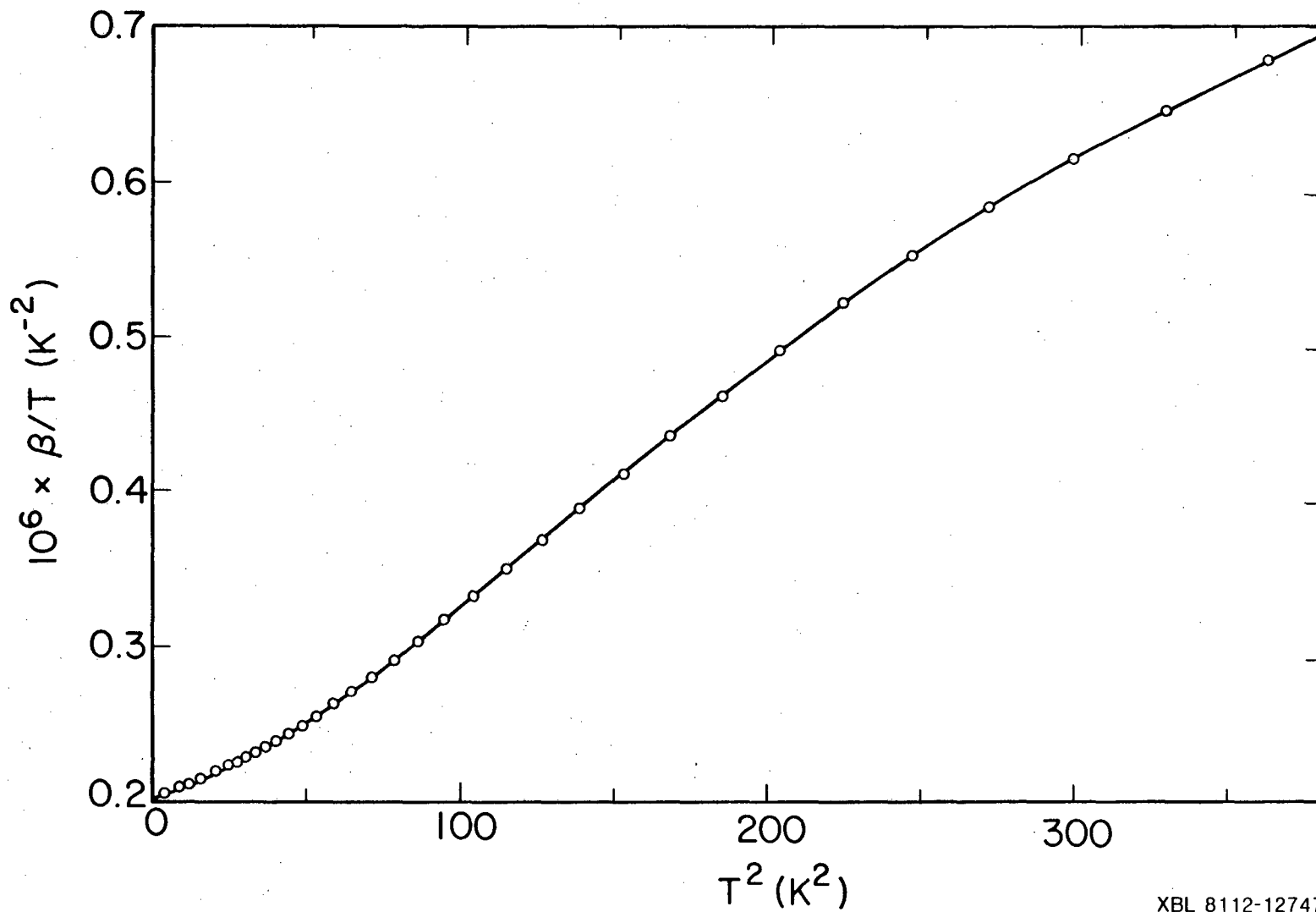


Fig. 12. The coefficient of thermal expansion for α -cerium derived from the pressure dependence of the heat capacity.

XBL 8112-12747

TABLE IV. Thermal Expansion Coefficient, $\beta = V^{-1}(\partial V/\partial T)_P$.^a

T (K)	$(\partial S/\partial \ln V)_T$ (mJ/mole-K)	$\beta \times 10^6$ (K ⁻¹)
2.0000	262.47	.4089
2.2014	290.04	.4519
2.4231	320.73	.4997
2.6670	354.76	.5527
2.9356	392.78	.6120
3.2312	425.37	.6783
3.5566	483.31	.7530
3.9147	537.74	.8379
4.3089	599.94	.9348
4.7427	671.47	1.046
5.2203	753.89	1.175
5.7460	850.22	1.325
6.3246	965.53	1.504
6.9614	1107.2	1.725
7.6624	1285.6	2.003
8.4339	1513.1	2.358
9.2832	1805.5	2.813
10.2179	2180.1	3.397
11.2488	2658.6	4.142
12.3793	3265.8	5.088
13.6258	4040.8	6.296
14.9979	5020.4	7.822
16.5081	6200.7	9.661
18.1704	7554.2	11.770
20.0000	9158.7	14.270

a. For $T < 2K$ use $\beta = (0.19958T + 0.001321T^3) \times 10^{-6}$.

$(C_p - C_v)/C$ is about 2×10^{-6} at 1K and 5×10^{-4} at 20K. This difference is negligible compared to experimental accuracy.

G. Magnetic Field Dependence

The specific heat of α -cerium varies only weakly with magnetic field if at all. Figure 13 displays the in-field data as relative deviations from a representative polynomial of the form $C(T) = AT + BT^3$. The beryllium-copper alloy from which the pressure cell was constructed contains enough magnetic impurities that the characterization of the addenda heat capacity as a function of magnetic field is less certain than as a function of pressure. The addenda heat capacity varied irregularly by as much as 15 percent as the impurity contributions to the heat capacity was shifted to higher temperatures with increasing magnetic field. Consequently, small differences in magnetic field seen at the pressure cell (due to changes in the positional relationship of the magnet and pressure cell from one experiment to the next) can lead to significant changes in the addenda heat capacity with respect to the cerium sample heat capacity. The temperature dependence of the observed field dependence of the heat capacity is similar in shape but much smaller in magnitude than that seen for the pressure cell alone. It is thus quite likely that only an apparent field dependence was seen (due to limitations on the accuracy with which the addenda heat capacity can be characterized). It is noteworthy, however, that the low field susceptibility measurements of Koskimaki and Gschneidner at low temperatures show positive curvature, i.e. $(\partial^2 \chi / \partial T^2)_H > 0$ and were independent of field in fields up to 1.3T

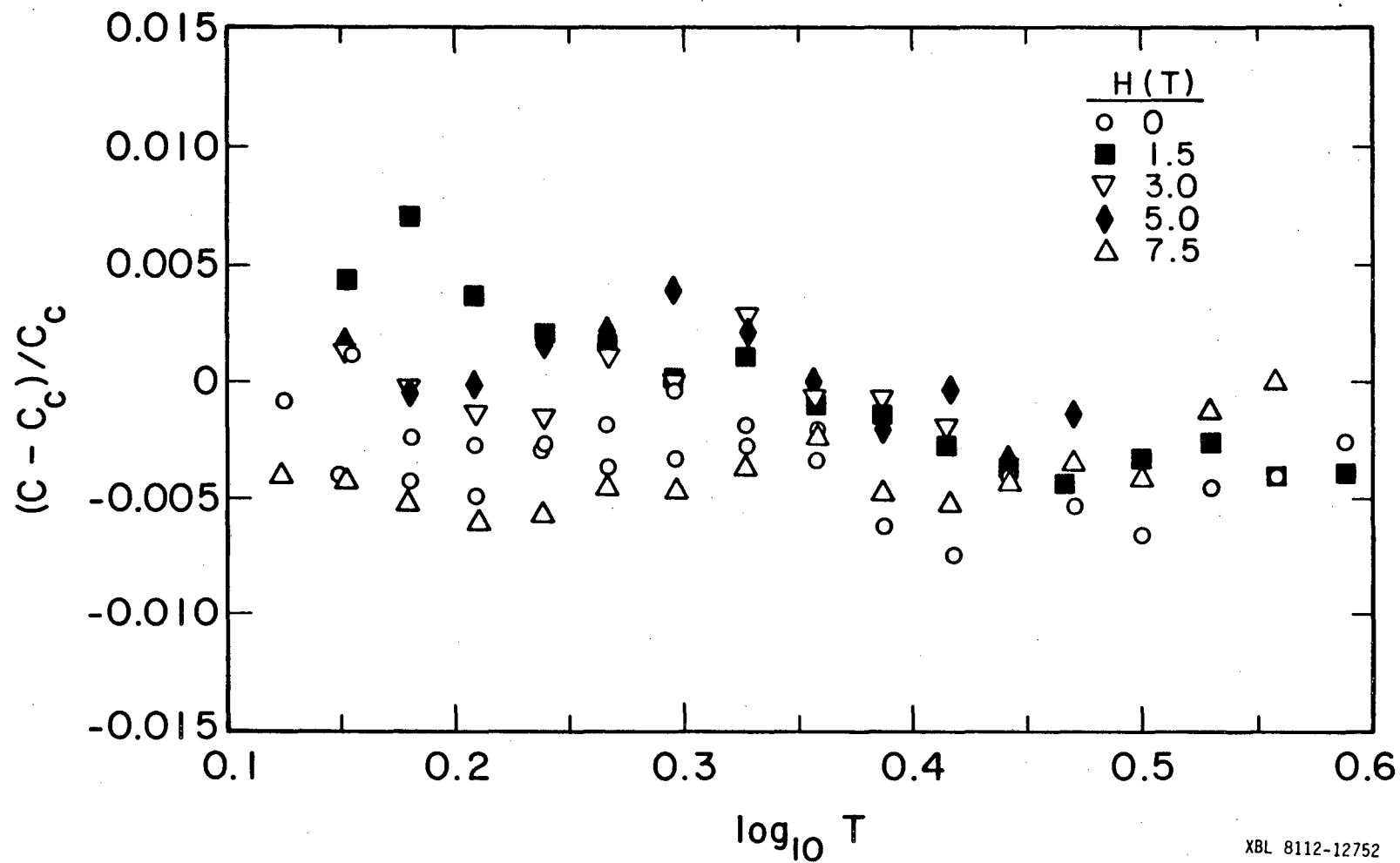


Fig. 13. The effect of magnetic fields on the heat capacity of α -cerium at 5.2kbar displayed as derivations from an arbitrary polynomial.

at temperatures of 1.8 and 4K.²⁷ It is therefore expected that $(\partial C/\partial H)_T > 0$ which is precisely the behavior observed at low field. Quantative comparison of the temperature dependence of the susceptibility and field dependence of the heat capacity would, however, require more precise heat capacity and susceptibility data, preferably from measurements on the same sample.

IV. DISCUSSION

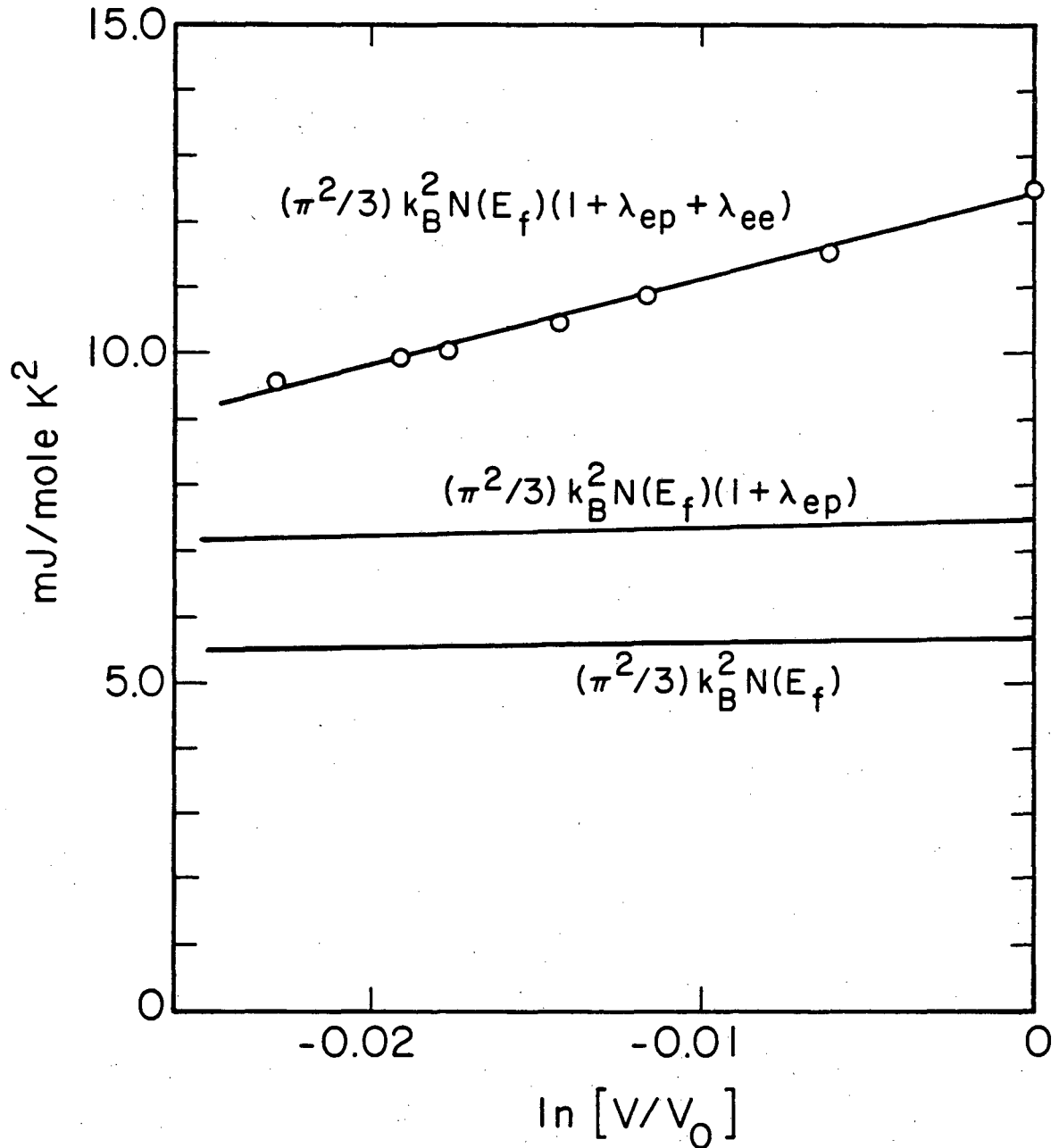
A larger volume dependence of the electronic specific heat coefficient, γ , was obtained from these experiments than suggested by earlier work.^{26,27} At a pressure of 9kbar, γ is depressed by 23 percent below its zero pressure value of 12.4 mJ/mole-K². For the range of pressures (0-9kbar) at which γ and θ_0 were measured experimentally, the volume dependence is well represented by the relations $\gamma = 12.34[1 + 10.38 \ln(V/V_0)]$ mJ/mole-K² and $\theta_0 = 179[1 + 2.58 \ln(V/V_0)]$ K, where V is the volume and V_0 is the zero pressure volume of α -cerium. Although not significantly different in the pressure range for which γ was measured, the relations $\gamma = 12.34(V/V_0)^{11.84}$ and $\theta_0 = 179 (V/V_0)^{-2.51}$ fit the data equally well, and give a weaker volume dependence in extrapolating to higher pressures.

Theoretical treatments of cerium fall into two categories, those for which the 4f electron delocalizes at the transition and those in which the localized 4f electron of γ -cerium is partially transferred into the sd conduction bands in the α phase. The recent band-structure studies of fcc cerium as a function of volume by Pickett et al. provide a means of comparing the experimental pressure dependence of γ with a delocalized 4f band picture of α cerium.²¹ These authors computed the electronic density of states at the Fermi level, $N(E_F)$, and the factor $\eta = N(E_F)\langle I^2 \rangle$, appearing in the McMillian decomposition of the electron-phonon enhancement factor $\lambda_{ep} = N(E_F)\langle I^2 \rangle / M\langle \omega^2 \rangle$, at five volumes ranging from that of γ -cerium at room temperature and zero

pressure to that of α -cerium at low temperatures and 15kbar. Only the smallest volume corresponds to a real state of α -cerium as the next smallest is about 0.66 percent larger than that of α -cerium at zero pressure. While $N(E_F)$ decreases by nearly a factor of two over the full range of these computations, the decrease is only 5.5 percent between the two smallest volumes. The theoretical values of $N(E_F)$ are too few and too widely spaced to accurately characterize its volume dependence, but since $N(E_F)$ is only weakly dependent on volumes a power law dependence was taken as the best available representation. A two point fit at the smallest volumes gives $N(E_F) = 32.96 (V/V_0)^{1.153}$ states/Ry, which corresponds to a 3 percent decrease for pressure increasing from 0 to 10kbar. Between the two smallest volumes for which it was calculated, η increases by 13 percent. A two point power law fit gives in this case $\eta = 0.899 (V/V_0)^{-2.90} \text{ eV-Å}^{-2}$, which implies a 7.8 percent increase for pressure increasing from 0.0 to 10kbar. The volume dependence of λ_{ep} is, however, much weaker as the increase in ω (which is proportional to ϵ_0) dominates in determining λ_{ep} and implies a decrease in λ_{ep} with decreasing volume. With $\epsilon_0 = 179 (V/V_0)^{2.51} \text{ (K)}$, and using the proportionality between ϵ_0 and ω given in Ref. 21, a power law representation of $\lambda_{ep} = 0.315 (V/V_0)^{2.12}$ is obtained. Pickett et al. reported $\lambda = 0.5$ at 15kbar using less accurate values of ϵ_0 to extrapolate to 15kbar. Their result, however, contains a numerical error in the calculation of $M_{\langle\omega^2\rangle}$ (given as 1.99 eV-Å^{-2}), which when corrected ($M_{\langle\omega^2\rangle} = 3.52 \text{ eV-Å}^{-2}$) gives

$\lambda_{ep} = 0.28$ at 15kbar. This corrected result is in agreement with Glötzel²⁰ who found $\lambda_{ep} = 0.3$ for $n = 1.0 \text{ eV-Å}^{-2}$ at zero pressure.

Figure 14 compares the experimental γ 's to the interpolations of the results of Pickett et al. discussed in the preceding paragraph. The pressure dependence of λ calculated from the phonon enhanced density of states is much weaker than that observed experimentally (4.5 percent decrease at 10kbar as opposed to 26 percent, respectively). Pickett et al. suggested that a small spin-fluctuation effective mass enhancement, λ_{sf} , may be important in γ and also in determining the superconducting transition temperature, T_c , of α -cerium. This enhancement would be additive, that is to say $\gamma = (2\pi/3) N_0 k_B^2 N(E_F) (1 + \lambda_{ep} + \lambda_{sf})$. If the discrepancies between the experimental results and band-structure calculations of γ are ascribed to λ_{sf} , then the latter decreases from 0.85 at 0.0kbar to 0.34 at 10kbar. Furthermore, λ_{sf} would appear to vanish near 20kbar if the extrapolations of γ , $N(E_F)$, and λ_{ep} by power law dependence on V are valid. Beyond 20kbar the extrapolation of γ falls below the extrapolated band-structure results. This is of course partly due to the disappearance of the λ_{sf} contribution, but may also indicate problems with these extrapolations or the band-structure results. The latter would not be surprising in that $N(E_F)$ is quite sensitive to the placement of the Fermi level, E_F , when the density of states has a steep slope near E_F as in α -cerium. For example, the band-structure results for α -cerium at zero pressure from the calculations of Glötzel²⁰ give a $N(E_F)$ which is 35 percent larger than that of Pickett et al. The volume dependence of $N(E_F)$ obtained



XBL 8112-12753

Fig. 14. Comparison of the experimental electronic specific heat coefficient (circles) with the bare density of states and phonon enhanced values from the calculations of Ref. 21. The factor λ_{ee} is the extra mass enhancement needed to account for the discrepancy between experiment and theory.

from a set of calculations using consistent approximations for each volume would, however, be less sensitive to the details of the bands. Assignment of the discrepancy between experimental and band-structure γ 's to a spin fluctuation contribution receives support from electrical resistivity measurements at low-temperatures as a function of pressure by Oomi.⁴⁴ A well defined T^2 term in the electrical resistivity was observed at low-temperatures. The coefficient of the T^2 terms was reduced to a third of its zero pressure value at 10kbar. This pressure-dependence is similar to that suggested for λ_{sf} by comparison of experimental γ 's with phonon enhanced density of state calculations of γ . Brinkman and Engelsberg⁴⁵ and Hertel, Appel, and Fay⁴⁶ studied the effect of magnetic field, H , on λ_{sf} and found that under special conditions (very low E_f , large Stoner enhancement S , and appreciable λ_{sf}) a field such that $\mu_B H$ is significant compared to E_f would reduce γ by a few percent. For α -cerium, however, E_f is large ($\sim 0.56Ry^{21}$) and S is modest (3.6^{21} or 5.8^{27}) and a field of about 3×10^3 T would be necessary to produce a noticeable effect. It is therefore not surprising that γ was field independent to within experimental resolution (about 1 percent for the in-field measurements).

The volume dependences of ϵ_0 , λ_{ep} , and λ_{sf} are also important in determining the volume dependence of T_c . Probst and Wittig found that in α -cerium, T_c was 20mK at 20kbar and increased to 50mK at 40kbar.⁴⁷ A straightforward calculation by the McMillian equation $T_c = \langle \omega^2 \rangle^{0.5} \exp[-1.04(1 + \lambda) / \lambda - \mu^*(1 + 0.62 \lambda)]$ which does not include λ_{sf} and with $\mu^* = 0.13$ yields $T_c = 20, 5, \text{ and } 2\text{mK}$ for pressures of $p = 0, 20, \text{ and } 40\text{kbar}$ respectively. While these T_c 's are in the low mK

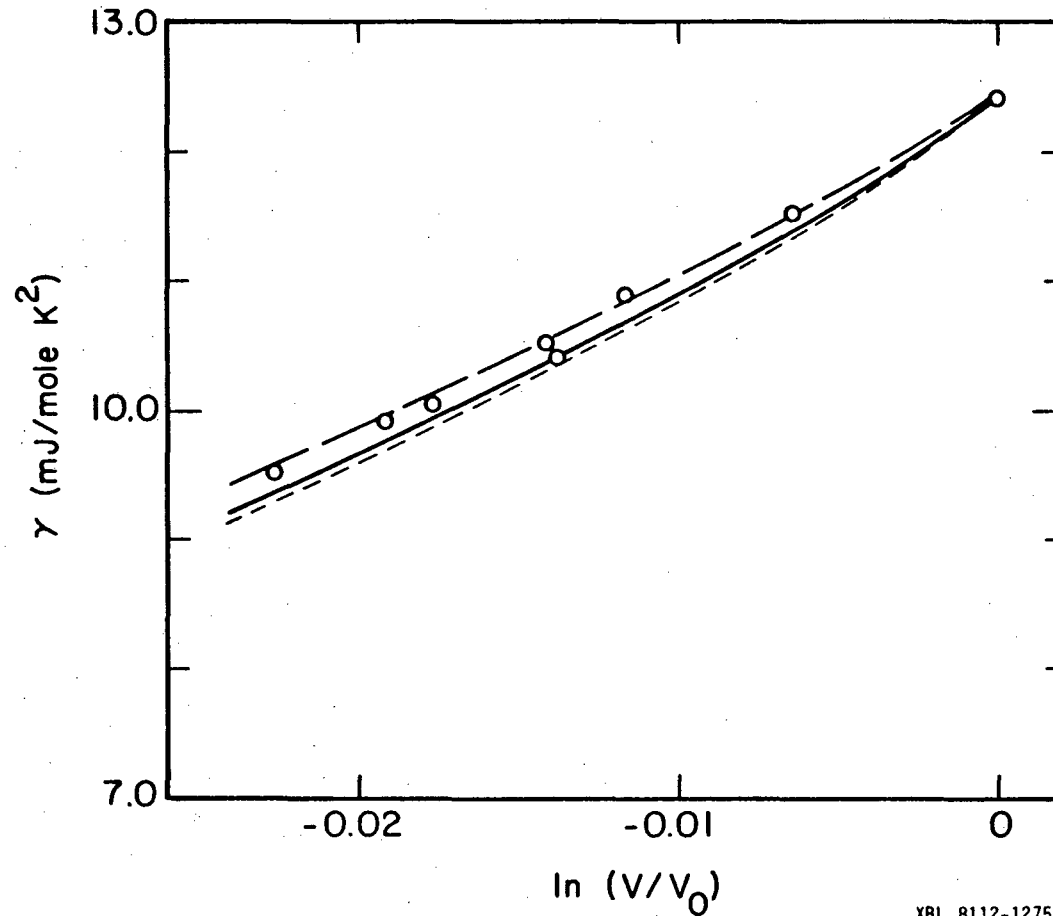
range appropriate for α -cerium, this calculation predicts the wrong sign for dT_C/dP . Wittig et al. suggested that the positive dT_C/dP might be due to phonon softening as the α - α' phase boundary is approached and that the minimum in the cerium melting curve might be indicative of this mode softening. Application of the Lindemann relation, $\theta \approx 200 V^{1/3} (T_m/M)^{1/2}$, gives $\theta = 207$ and $205K$ at 20 and $40kbar$ respectively. The change is, however, too small to account for the observed rise in T_C . The extrapolation of the experimental θ_0 's gives 201 and $215K$ at the same pressures, but would not be expected to give the correct results if phonon softening were occurring. Fitting of the McMillian T_C equation and the extrapolation of λ_{ep} from the results of Pickett et al. and the volume dependence of θ_0 from heat capacity experiments to the experimental T_C 's at 20 and $40kbar$ with $\mu^* = 0.13$ yields $\lambda_{ep} = 0.315$ and 0.340 and $\theta_0 = 179$ and $172K$ for those pressures respectively. These results show that phonon softening cannot be ruled out. Pickett et al. suggested (on the basis of a λ_{ep} which was in error) that λ_{sf} was responsible for the low T_C and also the positive dT_C/dP . Their explanation is reasonable, despite the error in λ_{ep} which led to that conclusion. An approximate equation was given as

$$T_C = (\omega_{log}/1.2) \exp[-1.04(1 + \lambda_{ep} + \lambda_{sf}) / \lambda_{ep} - \lambda_{sf} - \mu^*(1 + 0.62\lambda)] .$$

If λ_{sf} decreases more rapidly than λ_{ep} , then dT_C/dP would be positive. Quantitative comparison is impractical due to the sensitivity of this relation to the choice of λ_{ep} , μ^* , and λ_{sf} . If, however, λ_{ep} is

accepted to be uniformly low by 26 percent, then the experimental T_C 's at 20 and 40kbar are fit by $\lambda_{sf} = 0.028$ and 0.0 respectively with $\mu^* = 0.13$. Alternatively, if λ_{ep} is accepted as correct, then a $\mu^* = 0.08$ implies $\lambda_{sf} = 0.017$ and 0.0 for 20 and 40kbar respectively. In any case, a small pressure dependent λ_{sf} could override a decrease in λ_{ep} and lead to a positive dT_C/dP of magnitude comparable to the experimental value.

An alternative picture of α -cerium is provided by three promotional models of the γ - α phase transition. These are the virtual bound state (VBS) model of Coqblin and Blandin,⁵ the Ramirez and Falicov (RF) model⁶ as modified by Alascio, Lopez, and Olmedo to include hybridization between 4f and conduction band states,⁷ and the interconfigurational fluctuation (ICF) model of Hirst.⁸ Each of these models was successful in describing the major features of the γ - α cerium phase transition with only a few parameters. Moreover, the continued depopulation of the 4f states with increasing pressure in α -cerium implies a decrease in the electronic specific heat coefficient γ from this depopulation. Figure 15 compares the volume dependence of γ predicted by each of these (VBS, RF, and ICF) models to the experimental results. Agreement at zero pressure was forced by the choice of the sd conduction band density of states, $N_{sd}(E_F)$, or the 4f resonance width, Γ . In the original comparison of the theoretical prediction of γ resulting from these models,^{5,48,49} with available heat capacity data,^{22,23,26,27} the electron-phonon enhancement, λ_{ep} , was ignored. Here, this contribution is included with $\lambda_{ep} = 0.29$ for all three models



XBL 8112-12750

Fig. 15. Comparison of the experimental electronic specific heat coefficient (circles) with theoretical models: the ICF model (broken line),^{8,45} the VBS model (full line),⁵ and the extended RF model (dashed line).⁶

and is treated as volume independent. This approximation is consistent with the results of band-structure studies^{20,21} which have been discussed in detail. For each model $\gamma = (\pi/2/3) N_0 k_B^2 [N_{sd}(E_F) + N_f(E_F)](1 + \lambda_{ep})$, where $N_f(E_F)$ is the volume dependent 4f contribution to the electronic density of states at the Fermi level.

Olmedo, Lopez, and Alascio derive a low-temperature 4f occupation number, n_f , from a second order thermodynamic perturbation approach.⁴⁸ Their result is $n_f = 6 W_h / \pi T_0 (W_h + T_0)$, where T_0 is the energy of the 4f level and W_h is the energy of the bottom of the conduction band, both relative to the Fermi level. All energies are given in eV with $\Gamma = 0.02\text{eV}$, $W_h = -2.72\text{eV}$, and $T_0 = 0.118 + 0.00366P$, where P is the pressure in kbar. This parameterization of the 4f energy, which is nearly identical to that given for the original RF model in Ref. 6, was chosen to reproduce the γ - α cerium transition temperatures. The resulting n_f is consistent with valences assigned on the basis of other experiments in Ref. 4. Olmedo et al. gave $N_f(E_F) = n_f/T_0$. Using this expression for $N_f(E_F)$ and $N_{sd}(E_F) = 20Ry^{-1}$ as in Ref. 6, the results presented in Fig. 14 are obtained. Agreement in both the magnitude and pressure dependence of γ is excellent, but is perhaps due to the fortuitous choice of $\Gamma = 0.02$ eV.

The VBS model of Coqblin and Blandin also predicts a pressure dependent n_f and $N_f(E_F)$.⁵ The model has a Lorentzian $N_f(E_F) = 14 / \pi[\Gamma^2 + E_f^2]$, where Γ is the 4f resonance width and E_f is the 4f energy relative to E_F . The pressure dependence of $N_f(E_F)$ is not given explicitly, but is obtained by integration of $N_f(E_F)$ to obtain n_f and

then using the pressure dependence of n_f from the modified RF model which corresponds to estimated valences in α -cerium. The resulting $n_f = (14/\pi)[\tan^{-1}(E_f/\Gamma) + \pi/2]$ fixes the ratio E_f/Γ . A pressure independent $\Gamma = 0.0091\text{eV}$ gives good agreement with the experimental γ and its pressure dependence with $N_{sd}(E_f) = 20\text{Ry}^{-1}$ and $\lambda_{ep} = 0.29$ as in the treatment of the modified RF model. The results, $\Gamma = 0.0091\text{eV}$ and $E_f = 0.12$ to 0.16eV , are in good agreement with those used in the original treatment of the VBS model.⁵ It is not surprising that these two models agree since the pressure dependence of n_f was assumed to be identical and $N_f(E_f)$ reduces to $m/\pi E_f^2$ for $\Gamma \ll E_f$ or T_0 and $T_0 \ll W_h$. The different degeneracies, m , and the small difference between T_0 and E_f are compensated for by different Γ 's. The important point is that the pressure dependent n_f implied by other experimental evidence results in a pressure dependence of γ in excellent agreement with experimental heat capacity data.

The ICF model, like the VBS model, gives a Lorentzian $N_f(E_f)$.⁴⁹ In addition, this model assumes a weak volume dependence for $N_{sd}(E_f)$ given by $N_{sd}(E_f) = N_0(E_f)(V/V_\gamma)^{0.5}$ where $N_0 = 2.0\text{eV}^{-1}$ and $V_\gamma = 35.5\text{\AA}^3$ is the atomic volume of γ -cerium. The resulting value for α -cerium at zero pressure is $N_{sd}(E_f) = 24.4\text{Ry}^{-1}$ which is about 20 percent larger than that used in the VBS or modified RF models and its pressure dependence accounts for about 5 percent of the observed depression of γ at 10kbar. Hirst parameterizes n_f by the relations $n_f = 1-z$ and $dz/dV = \beta N_{sd}(E_f, V)$ with $n_f = 0.4$ for α -cerium at zero pressure and $\beta = 110\text{kbar}$. This n_f is about 23 percent larger than that used in the

VBS and modified RF model, but is the value necessary to fit the experimental cerium P-V-T relations. This model gives $N_f(E_F) = 2(1 - 5z)/\pi(1 + x^2)$ where $x = \tan[\pi(1 - 7z)/2(1 + 5z)] = 2E_f/\Gamma$.⁴⁹ Agreement with heat capacity data at zero pressure is obtained for $\Gamma = 0.106\text{eV}$ and $E_f = -0.163\text{eV}$, where $\lambda_{ep} = 0.29$ as in the treatment of the VBS and modified RF models. The pressure dependence of γ is in slightly better agreement with the experimental data than are the VBS or modified RF models. The better agreement results mostly from the choice of a larger $N_{sd}(E_F)$ which results in a broader $N_f(E_F)$ with a weaker volume dependence. The resonance width, Γ , for this model is, however, much greater than that of either the VBS or modified RF model.

The preceding discussion has shown that several promotional models of the γ - α cerium phase transition make excellent predictions for the volume dependence of the electronic specific heat of α -cerium. The electronic properties of α -cerium in these models are dominated by a narrow partially occupied 4f state extending to just below the Fermi level. Ratto, Coqblin and d'Agliano studied the effect of 4f electrons in cerium and lanthanum on the superconducting transition temperature, T_C , and obtained the result: $\ln(T_{CO}/T_C) = \alpha(7\pi n^2 + 2\pi n^3 \alpha)/(49\beta - 2\pi n^3 \alpha)$ where T_{CO} is the transition temperature with no 4f electrons, $n = n_f/2$, $\beta = N_{sd}(E_F)$, and $\alpha = \ln(1.14 \theta_0/T_{CO})$.⁵⁰ When this study was made, superconductivity had not been observed in α -cerium and α' -cerium was thought to be fully tetravalent α -cerium with $T_C = 1.5\text{K}$. The latter T_C was taken as T_{CO} for α -cerium. Then with $\Gamma = 0.01$ or 0.02eV and $\theta_0 = 158\text{K}$ theory predicted T_C for α -cerium as less

than the temperatures for which it had been studied experimentally. It is now known that α' -cerium is a different crystallographic phase. Consequently, the assumed $T_{C0} = 1.5\text{K}$ is inappropriate and must be determined by another means. The discovery of superconductivity in α -cerium and the determination of its pressure dependence provides experimental data⁴⁷ which can be fit to the model of Ratto et al.⁵⁰ The extrapolation $\theta_0 = 179 (V/V_0)^{-2.51}$ gives 201.3 and 214.3K at 20 and 40kbar respectively. Taking $\epsilon = 0.0091$ eV as suggested by comparison of heat capacity data with the VBS model and $n_f = 0.200$ and 0.149 at 20 and 40kbar as implied by the modified RF model, leaves only the single parameter T_{C0} free. Solving the equation of Ratto et al. with T_C and θ_0 appropriate for 20kbar, T_{C0} is found to be 91mK. Then at 40kbar, the relation of Ratto et al. gives $T_C = 41\text{mK}$ which agrees well with the experimental 50mK T_C considering both experimental uncertainty and the number and range of extrapolations involved.

The experimental electronic specific coefficient of α -cerium and its pressure dependence are in good agreement with predictions resulting from several promotional models of the γ - α cerium phase transition. While much other experimental data is also in agreement with these models, including the pressure dependence of T_C , other experiments, photoemission spectroscopy, positron annihilation, and Compton profile are in conflict with promotional models. Furthermore band-structure calculations predict that both γ and α -cerium have approximately one 4f electron and that the major change in electronic

structure is a broadening of the 4f band in α -cerium. The band-structure results agree well with most experimental data, but agreement with heat capacity results requires a pressure dependent spin-fluctuation enhancement, λ_{sf} . The existence of a pressure dependent λ_{sf} is supported by a T^2 term in the low-temperature electrical resistivity of α -cerium with a pressure dependence similar to that deduced for λ_{sf} from comparison of band-structure results with experimental heat capacity data. A pressure dependent λ_{sf} may also account for the large positive dT_c/dP in α -cerium. A theoretical study or a conclusive experimental determination of λ_{sf} and its pressure dependence is, however, necessary to bring the band-structure predictions into agreement with experimental heat capacity results. Nevertheless, when all experimental evidence is considered, it appears that the picture in which both γ and α cerium have one 4f electron, which is less localized in α -cerium, provides the best available description of cerium.

REFERENCES

1. D. C. Koskenmaki and K. A. Gschneidner, Jr., Handbook of the Physics and Chemistry of Rare Earths, K. A. Gschneidner, Jr. and L. Eyring eds. (North Holland, Amsterdam, 1978) Chapter 4, 337.
2. W. H. Zachariasen, quoted by A. W. Lawson and T. Tang, Phys. Rev., 76, 301 (1949).
3. L. Pauling, quoted by A. F. Schuck and J. H. Sturdivant, J. Chem. Phys., 18, 145 (1950).
4. K. A. Gschneidner, Jr. and R. Smoluchowski, J. Less Common Metals, 5, 374 (1963).
5. B. Coqblin and A. Blandin, Advan. Phys. 17, 281 (1968).
6. R. Ramirez and L. M. Falicov, Phys. Rev. B, 3, 2425 (1971).
7. B. Alascio, A. Lopez, and C. F. Olmedo, J. Phys. F: Metal Physics, 3, 1324 (1973).
8. L. L. Hirst, J. Phys. Chem. Solids, 35, 1285 (1974).
9. Y. Baer and G. Busch, Phys. Rev. Lett., 31, 35 (1973);
A. Platau and S. E. Karlsson, Phys. Rev. B. 18, 3820 (1978).
10. L. Brewer, Transition Metal Alloys: AIP Conference Proceedings Number 10, Section 1, H. C. Wolfe, editor (1973).
11. D. R. Gustafson, J. D. McNutt, and L. O. Roellig, Phys. Rev. 183, 435 (1969).
12. R. F. Gempel, D. R. Gustafson, and J. D. Willeberg, Phys. Rev. B 5, 2032 (1972).
13. U. Kornstadt, R. Lasser, and B. Lengeler, Phys. Rev. B 21, 1893 (1980).

14. D. Glötzel and R. Podloucky, *Physica* 102B, 348 (1980).
15. B. Johansson, *Phil. Mag.* 30, 469 (1974).
16. V. A. Shaburov, I. M. Band, A. I. Grushko, T. B. Mezentseva, E. V. Petrovich, Yu P. Smirnov, A. E. Soventnov, O. I. Sumbaev, M. B. Trzhaskavskaya, and I. A. Markova, *Zh. Eksp. Teor. Fiz.* 65, 1157 (1974) [*Sov. Phys. JETP*, 38, 573 (1974)].
17. B. D. Rainford, B. Buras, and B. Lebech, *Physica* 86-88B, 41 (1977).
18. C. Stassis, C. K. Leong, G.R.K. Kline, O.D. McMasters, and K. A. Gschneidner, *J. Appl. Phys.* 49, 2113 (1978).
19. C. Stassis, H. W. Deckman, B. N. Harmon, J. P. Desclaux, and A. J. Freeman, *Phys. Rev. B* 15, 369 (1977).
20. G. Glötzel, *J. Phys. F: Metal Physics* 8, L163 (1978).
21. Warren E. Pickett, A. J. Freeman, and D. D. Koelling, *Phys. Rev. B* 23, 1266 (1981).
22. O. V. Lounasmaa, *Phys. Rev.* 133, A502 (1964).
23. N. T. Panousis and K. A. Gschneidner, Jr., *Solid State Commun.* 8, 1779 (1970).
24. M. M. Conway, Ph.D Thesis, U.S. AEC Report No. LBL-827 (University of California, 1972).
25. D. C. Koskimaki, K. A. Gschneidner, Jr. and N. T. Panousis, *Journal of Crystal Growth*, 22, 225 (1974).
26. N. E. Phillips, J. C. Ho and T. F. Smith, *Phys. Lett. A* 27, 49 (1968).
27. D. C. Koskimaki and K. A. Gschneidner, Jr. *Phys. Rev. B* 11, 4463 (1975).

28. E. Franceschi and G. L. Olcese, Phys. Rev. Lett. 22, 1299 (1969).
29. E. S. Itskevich, V. F. Kraidenov, and V. S. Syzranov, Cryogenics, May 1978, 281.
30. A. Eichler and W. Gey, Rev. Sci. Instrum. 50, 1445 (1979).
31. P. F. Sullivan and G. Seidel, Phys. Rev. 173, 679 (1968).
32. N. M. Senozan, Ph.D Thesis, UCRL-11901 (University of California, 1965).
33. B. B. Triplett, Ph.D. Thesis, UCRL-19672 (University of California, 1970).
34. W. Fogle, to be published.
35. A. Jayaraman, A. R. Hutson, J. H. McFee, A. S. Coriell, and R. G. Maines, Rev. Sci. Instrum. 38, 44 (1967).
36. L. D. Jennings and C. A. Swenson, Phys. Rev. 112, 31 (1958).
37. T. F. Smith, C. W. Chu, and M. B. Maple, Cryogenics, Feb. 1969, 53.
38. Manufactured by Crystal-Solid State Divisin, Harshaw Chemical Co., Cleveland, OH.
39. W. T. Berg, Phys. Rev. B 13, 2641 (1976).
40. D. M. Newns and A. C. Hewson, J. Phys. F: Metal Phys. 10, 2055 (1974).
41. D. C. Koskimaki and K. A Gschneidner, Jr. Phys. Rev. B 10, 2055 (1974).
42. K. A. Gschneidner, Jr. and D. K. Thome, The Rare Earths in Modern Science and Technology, G. J. McCarthy and J. J. Rhyne eds. (Plenum, 1978) p. 75.
43. K. Andres, Phys. Rev. Lett. 10, 223 (1963).

44. Gendo Oomi, J. Phys. Soc. Jpn. 49, 256 (1980).
45. W. F. Brinkman and S. Engelsberg, Phys. Rev. 169, 417 (1968).
46. P. Hertel, J. Appel, and D. Fay, Phys. Rev. B 22, 534 (1980).
47. C. Probst and J. Wittig, Proceedings of the 14th International Conference on Low Temperature Physics, Otaniemi 1975, M. K. Krusius and M. Vierorio eds. (North Holland, Amsterdam, 1975) Vol. 5, p. 453.
48. C. F. E. Olmedo, Arturo Lopez, and B. Alascio, Solid State Commun. 12, 1239 (1973).
49. L. L. Hirst, Phys. Rev. B 15, 1 (1977).
50. C.F. Ratto, B. Coqblin, and D. Galleani d'Agliano, Advan. Phys. 18, 489 (1969).

PART TWO: A SEMI-AUTOMATIC LOW-TEMPERATURE
CALORIMETRY SYSTEM

I. INTRODUCTION

A. Semi-Automated Low-Temperature Calorimetry System

Low temperature calorimetry, which is a major source of information for the study of the properties of materials, demands a substantial investment of time and effort in data collection, workup, and analysis. As a practical consequence, both the number and scope of calorimetric investigations are limited. Automation, which does not necessarily reduce the time spent accumulating experimental data, can certainly reduce the manpower expenditure for the data collection and initial workup phase of an experiment. While automatic calorimetry at higher temperatures is common, only a few investigators have reported fully automated systems designed for operation in the liquid helium temperature region.¹⁻³ These systems have, in general, been limited in application to temperatures above 1K. Martin has extended automatic calorimetry to temperatures near 0.4K, but the instrumentation he uses and special problems encountered at low temperatures limit the overall precision of the experimental heat capacities to several percent. For many investigations, much greater precision is necessary to obtain useful results. For example, high precision is necessary when observing small changes in the heat capacity of a substance produced by varying an experimental parameter such as pressure, magnetic field, or, in the case of alloys, concentration. High precision is also necessary when a background heat capacity that is large relative to

the sample heat capacity must be subtracted from the total measured heat capacity to determine that of the sample.

At temperatures less than several K, high resolution adiabatic calorimetry encounters difficulties in the changing nature of important heat leaks, the rapidly diminishing heat capacity of many substances, and the frequent appearance of long internal time constants. While these problems prevent the reliable operation of an unattended fully automatic system, automated data collection, with on-line reduction, operated under close supervision, has much to offer. In addition to time and labor savings which may result, the opportunity to examine heat capacity data as they are accumulated permits the exercise of judgment in modifying the course of the experiment. For example, immediate availability of experimental heat capacities will indicate whether or not a change in magnetic field was sufficient to produce an observable change in heat capacity. Measurements near a feature in the heat capacity of a substance, such as might be associated with a phase transition, can be improved in that temperature increments can be adjusted as the data are taken to obtain the optimum compromise between accuracy and resolution. An additional benefit of automated data collection is that the algorithm used to reduce the raw thermometer output signals to temperatures has greater resolution due to signal averaging and provides improved point to point precision.

Automated systems have usually used mini-computers or remote hookup to large computer systems. The former have, in general, been prohibitively expensive when dedicated to a calorimetry system and the latter

has the disadvantage that real time computer control of the experiment is not usually practical and thus requires a separate data logging system. The development of powerful microprocessor based computers has made the design and use of a dedicated computer controlled instrumentation system more practical. Not only is the cost much less, but simpler logic and control signal timing has eased the task of interfacing a computer to a diverse array of instruments. For these reasons a microcomputer system was chosen for low temperature calorimetry data collection and analysis. Design considerations included retention or improvement of the accuracy and precision obtainable in manual heat capacity measurements, provision for the option of manual data acquisition if and when desirable, and use of existing instrumentation and techniques where possible. The system has been operational for several years and has been used for studies of dilute manganese in copper⁴ and of the pressure and magnetic field dependence of the low temperature heat capacity of α -cerium.⁵ In addition, by making large numbers of repeated measurements more practical, the system has proven useful in tracking down and eliminating several sources of error that have limited the reproducibility and accuracy of heat capacity data. An example of the latter was the determination that small quantities of hydrogen (used as a heat exchange gas in cooling from 77 to 20K), can be adsorbed onto the calorimeter and contribute a small and irreproducible component to the measured heat capacity. Moreover, the hydrogen adsorbed onto the vacuum can and can pumping line is apparently mobile enough that it can be re-adsorbed onto the calorimeter. These

effects were in some ways not surprising, but the relation between the magnitude of the consequent errors in heat capacity data and experimental conditions during cool down was more easily investigated with on-line data reduction. As a result, cooling is now either without exchange gas or the transfer of helium is stopped long enough to allow cold spots to warm sufficiently that the hydrogen can be more completely removed.

II. CALORIMETRY

The most general and accurate calorimetric method for use at low temperatures is the quasi-adiabatic heat pulse technique. In this method, the sample is attached to a small calorimeter or sample holder consisting of a mechanical support, a heater, and a thermometer. The sample and calorimeter are thermally isolated from their surroundings, usually by suspension from low thermal conductivity nylon or silk threads. A measured quantity of energy is introduced with the heater, and the change in sample temperature is monitored with the thermometer. The heat capacity of the sample C_s is obtained as $C_s = [Q/\Delta T] f_c - C_c$ where Q is the energy input, f_c is the "curvature correction" for the finite size of ΔT , derived from the temperature dependence of the measured heat capacity, and C_c is the calorimeter heat capacity, known from a separate measurement. The major disadvantages of this technique are its limited usefulness for small samples and the relatively large ΔT 's required to obtain acceptable precision and accuracy. Our automated system has been used with calorimeters optimized for operation over the 0.3-30K temperature range and samples with heat capacity comparable to one or two moles of copper. In general, precision is a little better than one-tenth of one percent and accuracy, which is limited by the accuracy of the temperature scale, is about one half of one percent. Addition of a second more sensitive thermometer to one calorimeter has permitted operation with a precision of a few hundredths of a percent over the 2-30K temperatures range. The automated calorimeter system is composed of three well defined but

tightly linked subsystems, the temperature measurement system, the energy control and measurement system, and the computer and its operating system which are described separately in the following sections. The overall system performance is evaluated in a final section.

III. TEMPERATURE MEASUREMENT SYSTEM

Our working thermometers for the 0.3–30K temperature range are all commercial encapsulated four-lead germanium resistance elements. Calibration of working thermometers is performed, in our laboratory, by comparison with two laboratory reference germanium thermometers. The reference thermometers are permanently mounted in a dedicated calibration apparatus designed for comparison of thermometers with the ^3He and ^4He vapor pressure temperature scales, a platinum resistance thermometer temperature scale, and a CMN magnetic susceptibility thermometry. Also mounted on the calibrator is an NBS SRM-767 fixed point device⁶ and another germanium resistance thermometer with a calibration traceable to the NBS 2-20K acoustic temperature scale.⁷ The working temperature scale is obtained by drawing a smooth curve through the residuals of a least square fit of the calibration data to a ten-term polynomial in $\log R$. For the automated calorimetry system, temperatures are obtained by interpolation from a dense table of approximately eight hundred points generated from the polynomial plus a correction from the smoothed residuals. Germanium resistance thermometers are useful for their ability to retain calibration through many thermal cyclings and over long time periods; however, to span the 0.3–30K temperature range and obtain a precision of 0.1 percent in heat capacity measurements, it is necessary to work with signal levels of a few hundred microvolts. For a typical low resistance germanium thermometer, a 10 percent temperature change results in a 20–80

microvolt change in thermometer voltage. Thermometer voltage resolution must therefore be a few hundredths of a microvolt to achieve heat capacities precise to a 0.1 percent.

Figure 1 is a block diagram of the temperature measurement system. The thermometer current source consists of a set of rechargeable NiCd cells regulated by a temperature controlled solid state voltage regulator and driving a low noise constant current source, a set of high precision standard resistors for current measurement, and a switching network for simultaneously reversing the thermometer current and potential leads. The solid state current supply provides current outputs ranging from 0.1 to 500 μ A in twelve steps of equal weight. Long term stability is better than 100ppm and short term stability is typically of the order of 10ppm/hour. The load rejection ratio $(\Delta I/I)/(\Delta R_L/R_L)$, is better than 10^{-6} which together with the high stability simplifies temperature measurement as only infrequent current measurement are necessary. The potentials across the standard resistor and the germanium thermometer are brought into a Leeds and Northrup 5556 six-decade potentiometer with a least significant dial step of 10 nV. The potentiometer has an internal switch matrix providing a digital readout of the potentiometer dial positions. The switch settings are encoded using simple TTL circuitry and read by the computer as directed. The potentiometer output signal is amplified by a Keithly Model 147 nanovolt null detector used as a high gain dc amplifier. The amplifier output is routed to a three-pole low-pass active filter and digitized by a twelve-bit analog to digital converter

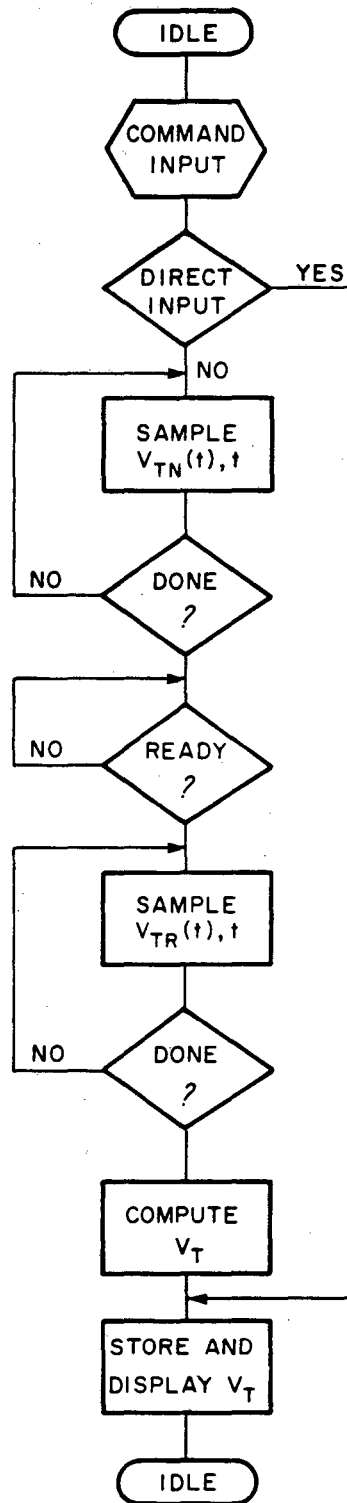
constructed from an integrated circuit DVM chip. With the amplifier gain set at 10^6 , the digitized potentiometer offset signal is resolved to about 3nV. The amplifier output is also routed through a two-pole passive low-pass filter attenuator to a recording potentiometer for visual display of the time dependence of the thermometer signal. The recording potentiometer trace is used to judge the steady state behavior of temperature drifts and is available for manual workup of calorimetry data if necessary.

The digitized potentiometer output is used with a real time system clock output to represent the time dependence of the thermometer signal as $V(t) = A+B(t)$ where the constants A and B are determined by a least-square fit. The low signal levels mandate careful treatment of spurious effects such as thermal emf's and zero-offsets generated in the circuit and accurate measurement of amplifier sensitivity. Amplifier sensitivity is sufficiently stable that measurement at the beginning of an experiment is adequate. Thermal emf's and zero-offsets are more dependent on environmental conditions and the usual practice is to measure each of them periodically during the experiment. The thermometer resistance, $R(t)$, derived from the thermometer current, I_T , potentiometer setting, E_p , the amplified potentiometer output, $V(t)$, the amplifier sensitivity, S , and corrections for zero-offset, V_z , and thermal emf's, V_T , is obtained as

$$R(t) = [E_p + S (V(t) - V_z - V_T)] / I_T .$$

The zero offset correction is defined as $V_z = [V_n(t_0) - V_r(t_0)] / 2$,

where $V_n(t_0)$ and $V_r(t_0)$ are obtained by evaluation of least square fits to the amplifier output with its inputs in the normal and reversed polarity configurations, respectively, as the temperature drifts. The thermal emf correction is similarly defined as $V_T = [V_{tn}(t_0) - V_{tr}(t_0)] / 2$ where $V_{tn}(t_0)$ and $V_{tr}(t_0)$ are evaluated from least square fits of the normal amplifier output and the output with both the potential and current leads to the thermometer reversed. The sensitivity is simply the change in potentiometer setting, ΔE_p , needed to produce an amplifier response, ΔV ; i.e. $S = \Delta E_p / \Delta V$, where $\Delta V = V_2(t_0) - V_1(t_0)$ is obtained from least square fits of the drifting amplifier signals. Figure 2 is a flow diagram illustrating the procedure for establishing the thermal emf correction. A similar sequence of actions serves to determine thermometer current, zero-offset correction, and sensitivity. The corrections V_T and V_Z are typically resolved to a few nV and their magnitude is usually less than $0.1 \mu V$. Thermometer currents are measured to 10ppm or better, depending on the magnitude of the current and the standard resistor used. Sensitivity measurements have a reproducibility of 0.3 percent when operating with an amplifier gain of 10^6 . Thus potential changes of less than 10nV are easily detected. This resolution and stability has proven adequate for obtaining heat capacities to better than 0.1 percent precision over the 0.3-30K temperature range using low resistance germanium thermometers.

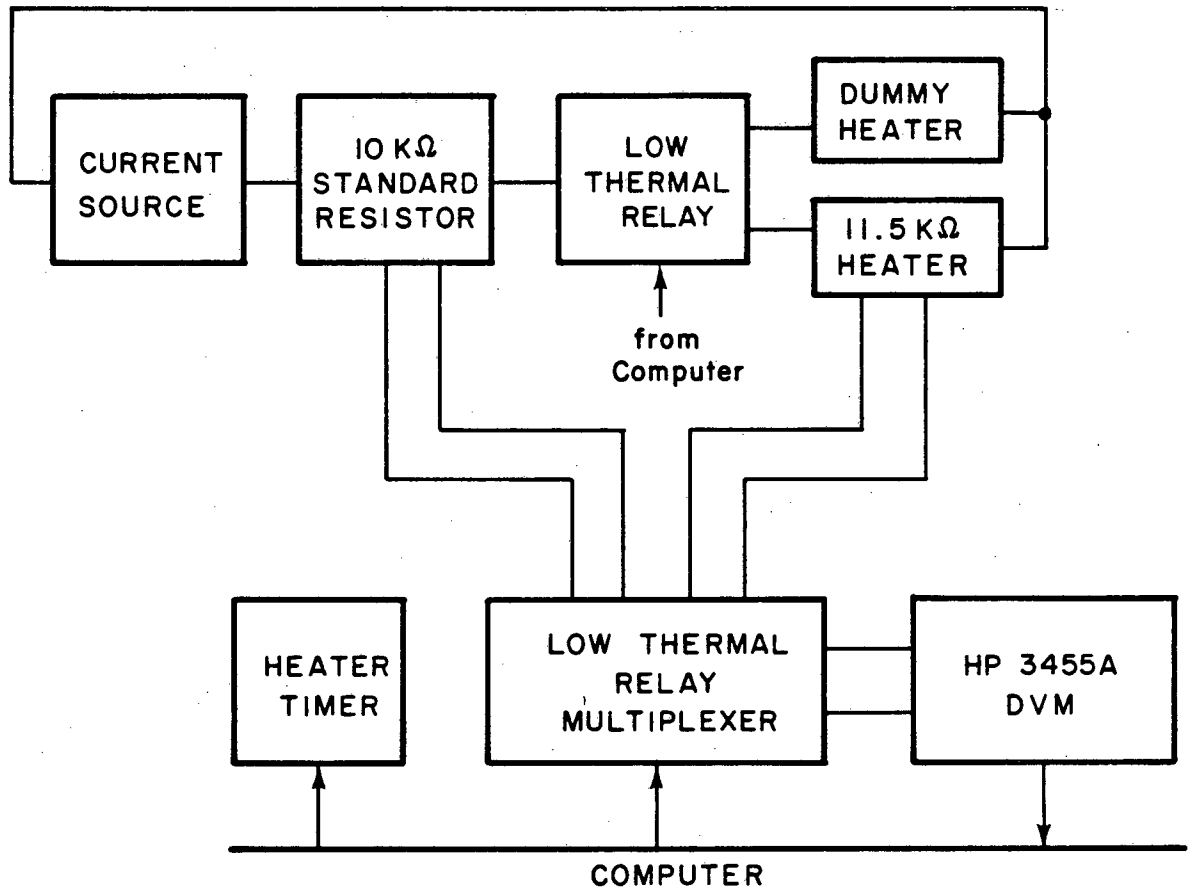


XBL 8112-12741

Fig. 2. Flow chart of the operations necessary for measurement of the thermal emf correction to the thermometer potential.

IV. ENERGY CONTROL AND MEASUREMENT SYSTEM

Energy measurement, which does not depend on the difference between small signals and for which the signal amplitudes are generally larger, is less demanding than temperature measurement. It has proven possible to completely automate the energy input and measurement phase of a heat capacity point. Figure 3 is a block diagram of the energy control and measurement system. The heater circuit resistance is very nearly time and temperature independent. Thus, a constant current can be obtained from a precision dc voltage standard providing a voltage output of 1-1000V. The total heater circuit resistance can be set to either $100\text{k}\Omega$ or $1\text{M}\Omega$ providing current ranges of either 0.01-10mA or 0.001-1mA. The heater current passes through a $10\text{k}\Omega$ precision standard resistor, used for current measurement, and is routed, by a low thermal reed relay under computer control, to either an adjustable dummy heater resistor or to the sample heater. The sample heater is wound non-inductively from 0.0009in. platinum-tungsten resistance wire and has a nominal resistance of $10\text{k}\Omega$. The heater pulse width is measured by a TTL counter driven by a 100kHz clock derived from the 2MHz system crystal controlled oscillator. The heater clock operates synchronously with the heat switch relay and has a resolution of 10^{-4} s and a range of about 840s. The accuracy of the heat pulse width determination is limited by uncertainties in heater relay opening and closing times to about 10^{-4} s, but is more than adequate for heat pulses longer than 1s. Two pairs of computer controlled SPST relays are used to multiplex the potential across the heater standard resistor or the heater



XBL 8112-12748

Fig. 3. Block diagram of the energy control and measurement system.

potential leads onto the input of an HP3455A 6-1/2 digit DVM. In the automated heater mode, the standard resistor potential is connected to the DVM immediately on closure of the heat switch relay and a one second settling time is allowed, after which the DVM is triggered for n measurements where $1 \leq n < 256$. The n DVM readings are averaged and the result is stored and displayed. A similar sequence is performed for the heater potential. The DVM is connected to the computer through its IEEE-488E interface. The DVM operating mode and range are automatically programmed by the computer. Measurements are triggered as needed by the computer. Stray RF power, introduced through the measuring circuit, limits the accuracy of the energy measurement at the lowest power levels. This stray power, which is measured by observing the change in the temperature of the sample and calorimeter produced by a heating period with the heater current source outputs shorted, has on occasion been as large as 5×10^{-9} W. Practically, this places a lower limit of 0.01mA on heater currents for short heat pulses when measuring the heater current and potential during the heating period. For lower power levels, the measuring circuit is disconnected and these are measured in a separate operation each time the heater current is changed. The stability of the heater current source and the low temperature coefficient of the heater resistance are such that the latter practice is more than adequate for 0.1 percent measurements of the energy input. In general, however, it has been possible to use the fully automatic energy measurement mode.

V. THE COMPUTER AND OPERATING SYSTEM

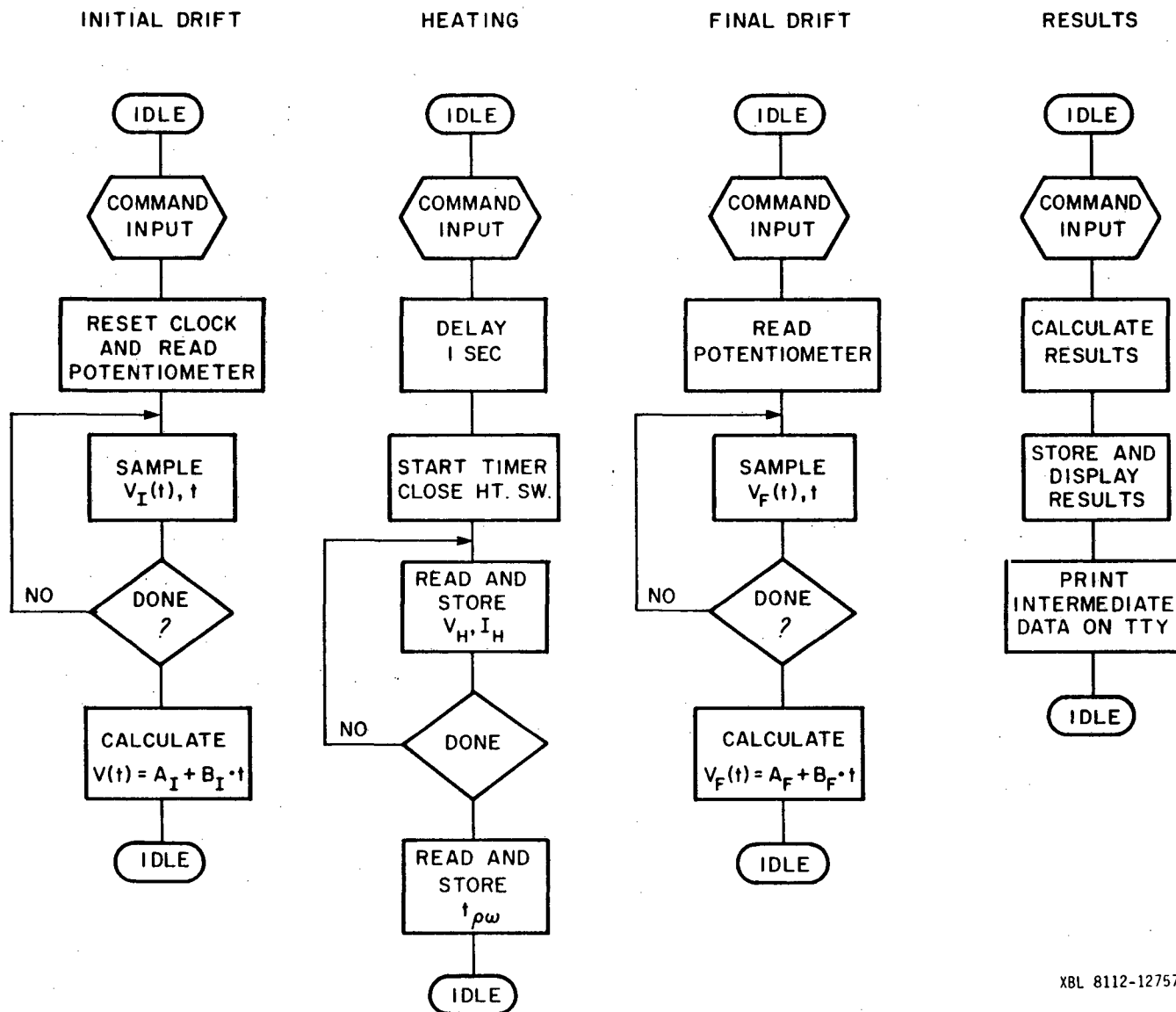
The computer system is based on the S-100 buss, a commercial semi-standard adopted by manufacturers catering to the computer hobbyist market. The foundation of this system is the definition of a one hundred connection backplane which interconnects modular system component such as the central processing unit, memory modules, and input-output modules. With the exception of specialized interfaces to the calorimeter instrumentation, most of the computer system is constructed from commercially built modules.⁸⁻¹² The system consists of a combined central processor front-panel, eight kilobytes of erasable read-only memory, forty kilobytes of read-write memory, and I/O interfaces. The central processor is built with an Intel 8080 eight-bit microprocessor operating on 500nsec cycle time. An integral octal front-panel allows loading and examining of cpu registers, memory, and I/O ports, and is useful for trouble shooting and testing system components. The eight kilobytes of read-only memory uses ultraviolet erasable electrically programmable memory chips and is used for permanent storage of frequently used programs. These programs consist of an assembly language based operating system and editor, routines for extended precision arithmetic, and an assortment of I/O device control programs. Forty kilobytes of read-write memory are used for storage of transient programs and data. The data stored in read-write memory includes tables for calculating temperatures and addenda heat capacities as well as experimental parameters and results. Computer I/O can be separated into an operator I/O group and instrument interface I/O

group. The operator I/O group consist of a typewriter style keyborad, a sixteen line by sixtyfour character alphanumeric CRT video display, a magnetic cassette tape data storage system, and a teletype printer. The operator enters command codes and data through the keyboard. Typed input is displayed on the CRT as typed and may be edited prior to execution of commands. The CRT also displays current values of important experimental parameters, prompting signals, and status messages. The magnetic cassette tape data storage uses audio frequency modulation for encoding digital data at about 120 characters per second. While somewhat slow, this facility provides useful permanant mass storage of programs and data. The teletype provides printed listings of selected raw data on a point by point basis and lists of data and processed results at the end of a series of experimental data points. The teletype paper tape punch can be used to transport experimental data to a large computer facility for further processing if necessary. The instrument interface I/O group provides communication between the computer and the temperature measurement and energy control and measurement systems and was described in Sections III and IV.

The operating system appears to the experimenter as a command oriented language. The operator types a one or two character command code followed by any necessary arguments. For example, entering the character string "E SR 1000 'CR'" causes the computer to assign the numerical value of 1000 to the variable "SR" which represents the value of the standard resistance used in measuring the thermometer current. In most cases, if a needed argument is not given, the last assigned

value is used. The computer acts on these command codes and prompts the operator when an external action, such as changing a switch position, is needed. Flexibility requires a large and versatile assortment of commands. Other than a few miscellaneous exceptions, commands fall into four major categories: data entry, process control, computation, and output. The data entry commands are used to define or change parameter values. In addition to a general purpose entry command, which references a parameter or variable by a symbolic name, there is a command causing a string of alphanumeric characters to be printed as a title heading each page of printed output and some of the process control commands permit input of specific parameters as arguments. The process control commands are used to direct the computer through data acquisition operations such as determining initial and final temperature drifts for a heat capacity point, determining corrections to the thermometer emf, and controlling energy input. Computation commands are used to initiate calculation of quantities such as temperature, addenda heat capacities, and total heat capacities. The data output commands produce printed listings of the data needed for heat capacity calculation, temperatures and calculated heat capacities, and corrections to calculated heat capacities, such as curvature correction and predefined addenda heat capacities. The available commands are briefly described in Section VI.

The flow charts of Fig. 4 illustrate the acquisition of a single heat capacity point. This operation is distributed over four separate command actions for convenience and flexibility. It is assumed that



83

XBL 8112-12757

Fig. 4. Flow charts for the four phases required for acquisition of a single heat capacity point.

the system parameters, thermometer current, system sensitivity, and thermal emf and zero offset corrections are defined. On receipt of the command code "ID", the real-time clock is reset and the setting of the potentiometer dials is read and stored. The amplified off-null signal from the potentiometer and the real-time clock are sampled. These quantities, $V(t)$ and t , are averaged over 2 to 32 readings for signal to noise enhancement. The resulting sampling rate ranges from eight samples/sec to one sample in two seconds. The sampled pairs are used to compute a running least square fit for $V_i(t) = A_i + B_i(t)$. Sampling continues until the experimenter, on judging the drift adequately characterized, terminates this phase from the keyboard. If the drift period was unsatisfactory for any reason, the initial drift phase is repeated; otherwise the heating phase is initiated by input of the command code "H". On receipt of this code, the program pauses for one second, while the operator reduces the amplifier gain. The heat switch is closed, the real-time clock sampled, and the heat pulse timer started. The potentials across the heater standard resistor and across the heater are measured and stored for computing the energy input. The heating phase continues until the experimenter determines that the change in temperature, typically $\Delta T \sim T/10$ or $T/20$, is adequate and terminates the heating period by keyboard input. The computer opens the heat switch, reads and stores the heat pulse width, t_{pw} , from the heater timer, and begins an idle state while the experimenter resets the potentiometer setting, increases the amplifier sensitivity, and waits for a steady state drift. The afterdrift phase

begins with input of the command code "OD", from the keyboard. This phase is much like the initial drift period except that the real-time clock is not reset. Sampling continues until the operator concludes that the drift is adequately characterized. This phase can be re-started if it is decided that steady state conditions had not been reached. The fourth and final phase, initiated by the command code, "C," begins with calculation of the results. The initial and final temperatures drifts, as characterized by the potentiometer output drifts, are evaluated at the midpoint of the heating period. Temperatures are obtained by a third order Lagrangian interpolation of a temperature calibration table. The heat capacity calculated as $C = I_H V_H t_{pw} / [T_2 - T_1]$ is assigned to temperature $T = 1/2[T_2 + T_1]$. The processed raw data E_I , E_F , I_T , I_H , V_H , and t_{pw} are stored in a data file and the quantities C , T , and ΔT are stored in a heat capacity file. The important system parameters are automatically printed on the teletype printer at the end of this phase. Queries from the keyboard produce CRT output for quantities such as $C_s = C_{tot} C_{add} - C_{sub}$, C_s/T , and T^2 for immediate examination or plotting.

Heat capacity data collected during a single experimental run are stored in an active file. At the end of a run, the file is processed further as needed. The raw data file containing the initial and final thermometer emf's, thermometer current, and heater current, voltage, and pulse width is printed on the teletype. This listing would be useful for reprocessing the data if the temperature scale definition were changed. The heat capacity data will usually need

correction for the finite size of the temperature increment. The correction is derived from a Taylor series expansion of an assumed power law temperature dependence of the heat capacity: i.e., $C = AT^X$. The correction is, to first order, $\Delta C/C = X(1-X)/24 (\Delta T/T)^2$, and amounts, for example, to 0.25 percent for $X = 3$ and $\Delta T = T/10$. A requirement for use of this correction is that any addenda heat capacities to be subtracted must have been similarly corrected before subtraction. A printed list of the curvature corrections, corrected heat capacities, and temperatures is available at the end of a run. The calorimeter heat capacity is represented in the program as a dense table of heat capacities. The relatively unstructured calorimeter heat capacity is characterized with accuracy of better than 0.01 percent with respect to assigned tabular values. Additional addenda heat capacities are represented as a sum of polynomials of up to twelve terms. These additional heat capacities can include contributions of varnish or grease used for improving thermal contact, or small amounts of pure materials used for minor modification of the calorimeter. The accuracy of the polynomial representation, must, of course, be judged on the basis of the material involved. A listing of heat capacities corrected for addenda contribution can be generated at the end of a run. If a mole number has been defined, the final resulting heat capacity is divided by this number, normalizing to a per mole or other basis. The listing includes total heat capacity, C_t , calorimeter heat capacity, C_c , miscellaneous addenda heat capacities, C_a , normalized heat capacity $C = (C_t - C_c - C_a)/\text{mole number}$, and the quantities C/T ,

T , and T^2 useful for graphical display of the data. This list of processed heat capacities can be generated more than once, using different addenda heat capacities or normalizing factors if desired.

VI. COMMAND CODE DESCRIPTIONS

A. Definitions

Commands, symbolic names, computer memory locations, and numerical values are represented as strings of keyboard symbols. In actual operation a space character separates these character strings, but for clarity quotation marks are added in the following text. The term "LOCATION" represents either a symbolic name or an absolute memory address in hexadecimal or decimal notation. The term "VALUE" refers to a real, integer, or logical constant depending upon the data type associated with the memory address at which it will be stored.

B. Data Entry Command Codes

"E" "LOCATION" "VALUE": This is the general purpose data entry command. The ASCII character string denoted by "VALUE" is evaluated and stored at the memory address implied by "LOCATION".

"TI" "TEXT": This command stores the ASCII characters symbolized by "TEXT" in memory. These characters serve as a page header on each printed page of teletype output. Maximum length is 72 characters.

"+" "ADDRESS": This command sets a pointer to an absolute memory address specified by "LOCATION." It is used in conjunction with the commands ":" and "?" to modify or edit data tables.

":" "VALUE": This command is used to load a real constant at the meaning address previously specified by a "+" command.

"R": This command loads a heat capacity file from magnetic tape for reprocessing.

C. Process Control Command Codes

"ID": This command is used to characterize the temperature drift prior to introduction of energy on taking a heat capacity point. It can be repeated indefinitely with only the last measured temperature drift used in computing the following heat capacity point. The initial drift phase is terminated by pressing the keyboard space bar.

"OD": This command is used to characterize the temperature drift following introduction of energy. The after drift phase is terminated by pressing the keyboard space bar. This command can also be REPEATED.

"H": This command begins the energy input phase of a heat capacity point. During this period the heater current and potential are normally automatically measured unless this function is disabled by the setting of a software flag. For both the current and potential a predefined number of readings are averaged. The resultant values are stored and displayed on the CRT. The energy input phase is terminated by pressing the keyboard space bar at which time the heat pulse width is read, stored and displayed on the CRT.

"S" "VALUE": This command is used to measure the amplifier sensitivity. The amplifier output for a given potentiometer setting is sampled as a function of time and the results fit to $V_i(t) = A_i + B_i(t)$. Sampling continues until the keyboard space bar is pressed. The operator changes the potentiometer dial setting and presses the return key. The amplifier output is again sampled and fit to $V_f(t) = A_f + B_f(t)$. Pressing the space key terminates this measurement and the sensitivity is calculated, stored in memory, and displayed.

The sensitivity, S , is defined as $E_p/\Delta V$ where ΔE_p is the change in potentiometer dial setting in microvolts and $\Delta V = V_f(t_m) - V_i(t_m)$ in volts. If a numerical value is entered with this command code that value is taken as the sensitivity.

"T" "VALUE": This command is used to define or measure the thermal emf correction to the thermometer potential. This correction is assigned the numerical value "VALUE" if a number follows the command code "T". Otherwise, the amplified potentiometer output is sampled as a function of time until the space key is pressed. The operator reverses the thermometer current and potential leads and presses the return key. The new thermometer potential is sampled until the space key is again pressed. The thermal emf correction V_T is calculated as $\Delta V/2$, stored in memory, and displayed on the CRT.

"0" "VALUE": This command is used to define or measure this zero offset correction to the thermometer potential. The correction is assigned the numerical value "VALUE" if a number follows the command code "0". Otherwise, the amplified potentiometer output is sampled as a function of time until the space key is pressed. The operator reverses the potentiometer output polarity and presses the return key. The reversed amplified potentiometer output is sampled until the space key is again pressed. The zero offset correction V_Z is calculated as $(V_n + V_r)/2$, stored in memory and displayed on the CRT.

"I" "SEN": This command is used to measure thermometer current. The potential across the thermometer standard resistor is brought into the potentiometer and nulled to the nearest microvolt.

The optimal argument "SEN" specifies the nominal amplifier sensitivity and has a default value of $3\mu\text{V}/\text{V}$. The off-null signal is sampled in normal and reversed polarity at sixteen samples for each configuration. The signals are averaged, multiplied by the nominal sensitivity, and added to the potentiometer dial setting. The result is divided by the value of the standard resistance yielding the thermometer current in μA which is stored and displayed on the CRT.

"MH" This command is used to measure the heater current and potential when measurement of these quantities would disturb the heater power during a true heating period. The measurement is identical to that normally performed automatically during the heat pulse.

">": This command turns the heater on manually.

"<": This command turns the heater off manually.

"K": Deletes last calculated heat capacity point from the data files and decrements point count and is used for the elimination of incorrect data.

D. Computation Command Codes

"C": This command is the final command in a heat capacity point operation. It causes calculation of the initial and final temperature, average temperature, temperature increment ΔT , the total heat capacity, C_t , addenda heat capacity C_{add} , the result $C = C_t - C_{\text{add}}$, and $C//T$. The important parameters are stored in memory and printed on the teletype for each point.

"F": This command causes a "curvature correction" to be computed for each point within an experimental run. The corrected heat capacities, fractional corrections, and temperatures are printed.

"TP": This command initiates calculation of the current temperature based upon the amplified potentiometer output, potentiometer dial setting, and previously measured thermometer current, sensitivity, zero offset, and thermal emf values. The resultant temperature is displayed on the CRT.

"T*": This command causes repeated interaction of the "TP" command and is terminated by pressing the "CTRL A" key.

"§": This command causes the heat capacity to be calculated from the currently stored parameters which may have been entered manually from the keyboard.

"!" "VALUE": This command initiates calculation of the addenda heat capacity at either the optional input temperature "VALUE" or from the last value assigned to the temperature.

E. Data Output Command Codes

"D": Produces a printed list of initial and final thermometer potentials and currents, the heater potentials and currents, and the heat pulse widths for the data points accumulated in the current experiment.

"L": Produces a printed list of the heat capacities, mean temperatures, and temperature increments for the points in the current experiment.

"A": Produces a printed list of the total heat capacity, addenda heat capacity, sample heat capacity, sample heat capacity divided by the temperature, temperature, and the temperature squared.

"W": Writes a copy of the heat capacity file on magnetic tape for long term storage.

F. Miscellaneous Command Codes

"RS": Resets point count and clears heat capacity data files.

"X": Exits from heat capacity program to operating system.

VII. SYSTEM PERFORMANCE

The automated data acquisition system with on-line data reduction has been used in calorimetric measurements for several years. Two major investigations, one of which required an extensive series of calibrations, have demonstrated the ability of the system to produce results of excellent precision and reproducibility. Point to point precision for a single run has often been nearly a factor of five greater than obtained in manual workup of the chart record. That is to say, the scatter of individual data points around a smooth curve is often less than a few-hundredths percent for an experiment which would be expected to produce 0.1 percent precision with manual workup. While this increased precision is useful, repeated runs usually achieve reproducibility only to within the expected 0.1 percent figure. For an exceptional experiment, using a high resistance germanium thermometer containing a small pressure of helium heat exchange gas, precision and reproducibility of 0.01 percent were obtained. The rapidly increasing resistance of this thermometer at low temperature and the input characteristics of the Keithly nanovolt amplifier reduces its usefulness below 2K. Consequently, most experiments have been limited to precision and reproducibility of slightly better than 0.1 percent and an overall accuracy of a few tenths of a percent. The automated system has proven useful in reducing the work needed to acquire large quantities of calorimetric data. The time required to characterize the temperature drifts and increment the sample temperature are about the same, both with and without the automated system.

Without the automated system, however, heat capacities are obtained only after tedious analysis of chart recorder traces. As the latter task is often the most time consuming, time and labor savings have proven valuable and become more so as the quantities of data collected increase.

REFERENCES

1. Douglas L. Martin, L. L. T. Bradley, W. J. Cazemier, and Robert L. Snowdon, Rev. Sci. Instrum. 44, 675 (1973).
2. R. E. Schwall, R. E. Howard, and G. R. Stewart, Rev. Sci. Instrum. 46, 1054 (1975).
3. Douglas L. Martin, Rev. Sci. Instrum. 46, 1670 (1975).
4. William E. Fogle, James D. Boyer, Norman E. Phillips, and John Van Curen, Phys. Rev. Lett. 47, 352 (1981).
5. Heat capacity of α -Ce, to be published.
6. J. F. Schooley, R. J. Soulen, and G. A. Evans, NBS Special Publication 260-44 (U.S. GPO, Washington D.C. 20402, 1972).
7. CryoCal No. 2776 purchased from Cryocal Inc., Riviera Beach, Fla.
8. Mother Board (backplane) and keyed up 8080 (cpu front-panel) from Thinker Toys, 1201 10th St., Berkeley, CA 94710.
9. Three eight-kilobyte read-write memory modules, by Bill Godbout Electronics, Box 2355, Oakland Airport, CA 94614.
10. Two eight-kilobyte read-write memory modules from Advanced Computer Products, P. O. Box 17329, Irvine, CA 92713.
11. Eight-kilobyte read-only memory module from Advanced Computer Products, P. O. Box 17329, Irvine, CA 92713.
12. VDM-1 Vidio Display Module by Processor Technology (defunct).

PART THREE: PRESSURE DEPENDENCE OF THE LOW-TEMPERATURE
HEAT CAPACITY OF TEFLON

I. INTRODUCTION

The pressure dependence of the low-temperature heat capacity of polytetrafluoroethylene (teflon) was measured for the purpose of determining the suitability of teflon as a pressure transmitting medium in high-pressure low-temperature calorimetric studies of metals. Teflon was found to be a poor choice for that application as the pressure dependence of its substantial heat capacity was not only very large but also very temperature dependent. The pressure dependence of the heat capacity of teflon is, however, quite interesting in itself due to the considerable interest in the heat capacity of amorphous and partially amorphous materials. These materials share two common characteristic features in their low-temperature heat capacities. In particular, all of them show a large excess over the T^3 Debye value predicted from acoustic measurements¹⁻³ and at low enough temperatures many show a contribution which is nearly linear in temperature.⁷ For polymers the heat capacity is reasonably well described by the Tarasov model,⁹ which represents the vibrational spectrum as a three dimensional continuum at low frequencies and a one dimensional continuum at higher frequencies, plus an additional contribution (the excess low-temperature heat capacity) arising from one or more sharp peaks in the low frequency phonon spectrum. The excess heat capacity contribution, which shows up as a rounded maximum at a few K when C/T^3 is plotted versus T or T^2 , is frequently represented by one or

more Einstein heat capacity functions with characteristic temperatures C/T^3 , θ_{E2} , etc. In polymers, the magnitude of this maximum depends strongly on crystallinity and crosslinking,^{1,4,6,7} but its position is relatively insensitive to these parameters. Most speculations on the origin of the excess heat capacity are related to the idea of vibrations of pendant groups near voids as suggested by Rosenstock.¹⁰ An important point, often overlooked, however, is that the excess over the Debye heat capacity is characteristic of amorphous materials in general and most likely originates from some common feature rather than structural details such as side groups of particular polymers. Compression of a polymer with high pressure increases its density without the introduction of extra material as does crosslinking and also permits heat capacity measurements on the same sample at different densities, which is impossible by variation of crystallinity and crosslinking. Heat capacity studies as a function of pressure are therefore useful for investigating the nature and behavior of the excess heat capacity.

II. RESULTS AND DISCUSSION

The experimental techniques used in this study are similar to those described in Section II of part one. The heat capacity of 0.1771g of teflon was measured at five pressures in the order 5.2, 3.5, 0.3, 0.8, and 1.6kbar. Data were taken for the temperature range 0.4–20K, but only those data above 1K are useful as the addenda heat capacity contributed more than 99 percent of the total below 0.8K. Above 1K the precision and accuracy of the teflon heat capacity rapidly improves to a few percent. The crystallinity of the sample is estimated to be about 62 percent from comparison of the density ($2.175\text{g}\cdot\text{cm}^{-3}$) to the densities of completely amorphous and crystalline teflon respectively.¹¹ The heat capacity data for teflon are displayed in Fig. 1 plotted as C/T^3 versus T^2 . The heat capacity, C_V , of teflon has a large maximum in C/T^3 at low temperature (which could be associated with an unusually large T^5 term). This maximum is, however, characteristic of amorphous materials for which extrapolation of C/T^3 to $T = 0\text{K}$ yields a T^3 coefficient 20–50 percent larger than implied by acoustic measurements. Figure 1 also illustrates the strong and temperature dependent pressure dependence of C_V . The temperature at which the maximum occurs increases from about 2.8K at 0.3kbar to near 4.5K at 5.2kbar while the magnitude of C_V decreases by almost a factor of two near the maximum. At temperatures much greater than that at which the maximum in C/T^3 occurs, the pressure dependence is much weaker and C_V decreases only about 15 percent between 0.3 and 5.2kbar. The relatively smooth variation of

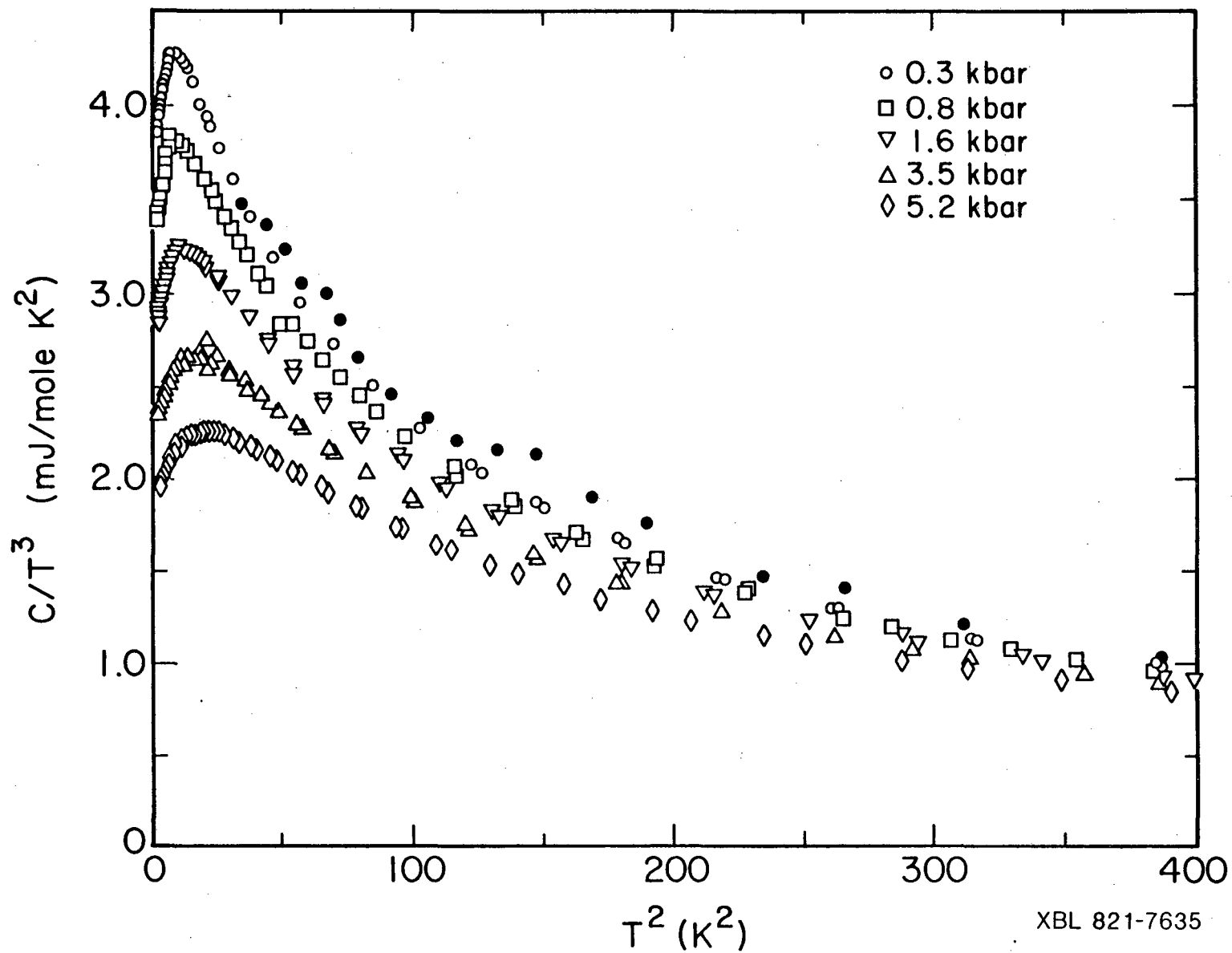


Fig. 1. Heat capacity data for teflon at five pressures. The solid circles represent the data of Choy et al.⁵

XBL 821-7635

C_V with pressure shows that there is no important hysteresis with pressure. The zero pressure data of Choy et al. on a different teflon sample are shown for comparison.⁵ Figure 2 displays the low temperature data on an expanded scale to illustrate the low-temperature behavior. There is a small upward trend in the data at the lowest temperatures for the two highest pressure runs where the excess in C_V has been largely suppressed. This upturn could be due to a linear contribution to C_V like that usually seen in amorphous materials at low enough temperatures. For the 5.2kbar run, the data suggest a linear term with a coefficient of about 0.05 mJ/mole-K² which is comparable to that seen in amorphous SiO₂, GeO₂ and Se.¹² The precision and accuracy of the low-temperature data are, however, too poor to permit quantitative characterization of the magnitude or pressure dependence of a linear term.

The data were characterized by fitting to a model for which C_V is the sum of a Tarasov term, C_T , plus two Einstein heat capacity functions $n_1 C_{E1}$ and $n_2 C_{E2}$ with characteristic temperatures θ_{E1} and θ_{E2} and numbers of modes n_1 and n_2 respectively. An attempt to fit the data with $C_V = C_T + n_1 C_{E1}$ was entirely unsuccessful. The Tarasov contribution is given by $C_T/4R = D_1(\theta_1/T) - (\theta_3/\theta_1)[D_1(\theta_3/T) - D_3(\theta_3/T)]$ where D_1 and D_3 are the one and three dimensional Debye functions. The characteristic temperature θ_3 defines the cutoff frequency of a three-dimensional continuum and the beginning of a one-dimensional continuum extending up to θ_1 . The factor 4 multiplying R associates four elastic modes with each repeat unit

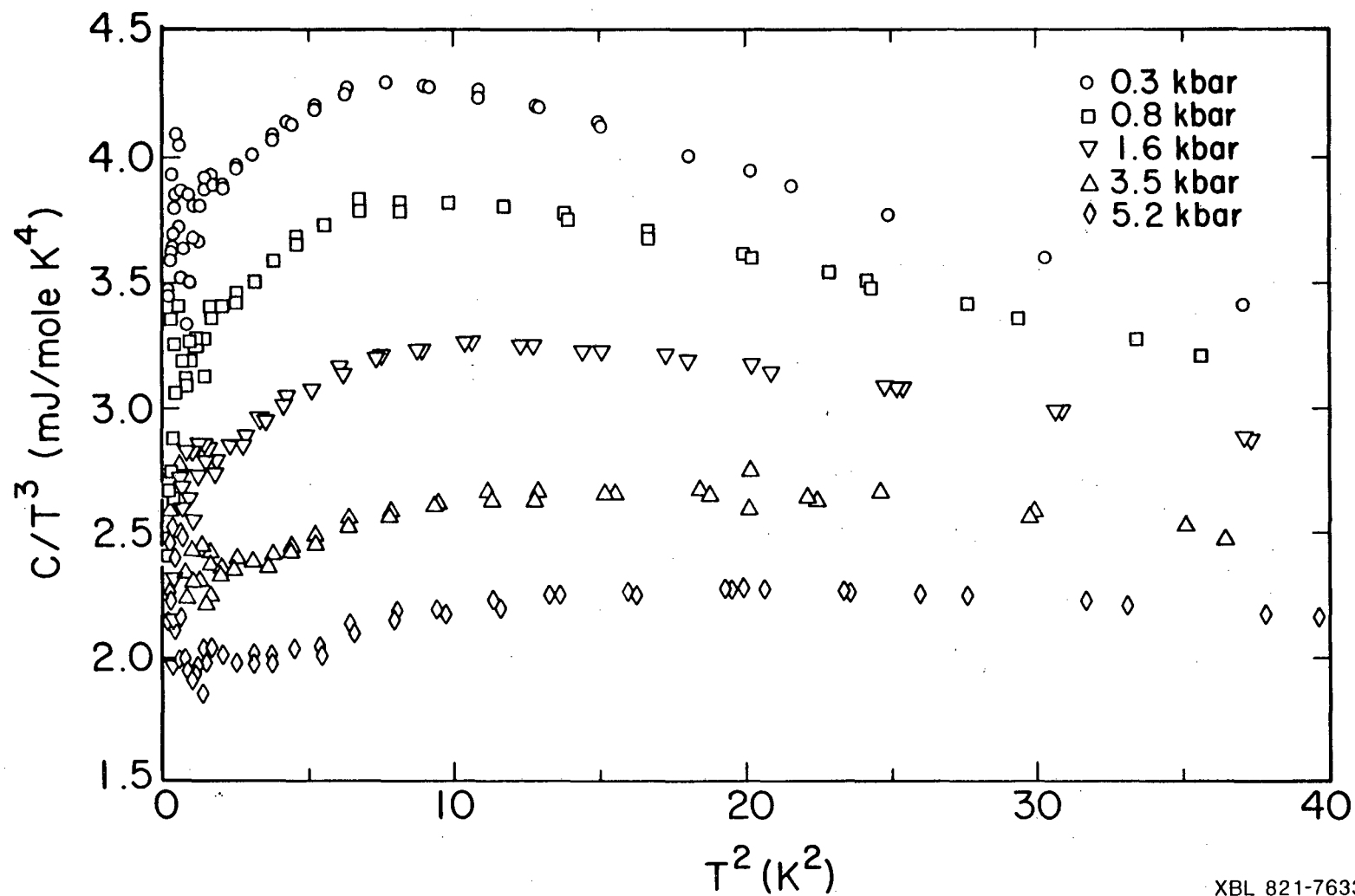


Fig. 2. Heat capacity data for teflon on an expanded scale.

(C_2F_4) and assumes that the carbon-carbon vibrational modes appear in optical branches.¹³ The low temperature limit of C_T/T^3 is $16\pi^4 R / (5\theta_1\theta_3^2)$. The fitting procedure found most effective was to subtract the excess heat capacity, $C_{EX} = n_1 C_{E1} + n_2 C_{E2}$, from C_V while varying n_1 , n_2 , θ_{E1} , and θ_{E2} such that the remainder (which is simply C_T) when plotted as C_T/T^3 versus T^2 was constant for $T^2 < 20K^2$ and decreased at higher temperatures as appropriate for a Tarasov model. This procedure was quite sensitive to the choice of the parameters n_1 , n_2 , θ_{E1} , and θ_{E2} and variation of any of them by more than a few percent resulted in pronounced structure in C/T at low temperature. It was found that n_1 and n_2 determined from the 0.3kbar run, for which C_{EX} is most significant, produced the best fits at other pressures. This implies that n_1 and n_2 are relatively pressure independent. The low-temperature limit of $(C_V - C_{EX})/T^3$ is 2.88 mJ/mole-K^4 which compares well with the value 2.81 mJ/mole-K^4 calculated from sound velocity measurements on a different teflon sample at zero pressure.¹⁴ Figure 3 shows the successive subtractions of the two Einstein terms and compares the remainder to a Tarasov heat capacity. The remainder $C_V - C_{EX}$ was fit to a Tarasov model by noting that the low-temperature limit of C_T/T^3 determines $\theta_1\theta_3^2$ and separating this product by choosing θ_1 and θ_3 such that $C_T = C_V - C_{EX}$ at 20K. The table of $D_1(\theta/T)$ compiled by Wunderlich was used to calculate the D_1 contributions to C_T .¹⁵ The resulting fit represents the experimental data to within 5 percent over the 1-20K temperature range. A non-linear least-square fitting procedure would produce a better RMS deviation than use of a single

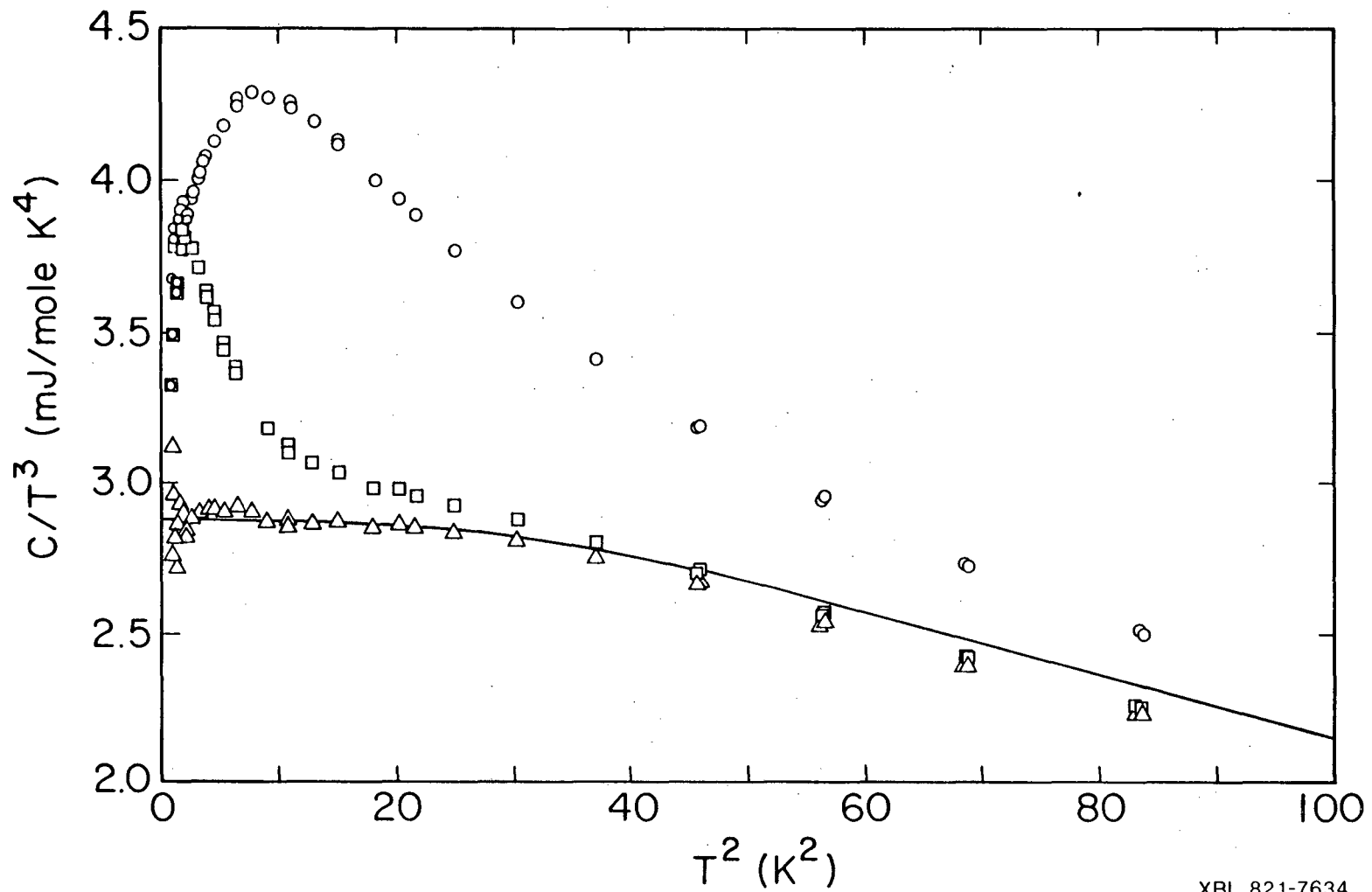


Fig. 3. The 0.3kbar heat capacity data showing the successive subtraction of two Einstein heat capacity functions. The solid curve represents a fit to a Tarasov model.

value of $C_V - C_{EX}$ to separate θ_1 and θ_3 , but is impractical due to the difficulty of representing $D_1(\theta/T)$.

Figure 4 shows the pressure variations of θ_1 , θ_3 , θ_{E1} , θ_{E2} relative to their respective 0.3kbar values and numerical values of these parameters are given in Table I. Varying any of these parameters by more than 5 percent results in a much poorer fit and therefore 5 percent is taken as an estimate of their uncertainty. Both θ_{E1} and θ_{E2} increase strongly and linearly with P . This accounts for the increase in the temperature at which the maximum in C/T^3 occurs and also the broadening of the maximum at higher pressures. The constant values of n_1 and n_2 show that the entropy associated with C_{EX} is not removed by application of pressure but only shifted to higher temperatures. Both θ_1 and θ_3 also increase with pressure, but much less drastically. While the variation of θ_1 and θ_3 with pressure, P , is relatively smooth, it is not linear in P , $\ln P$, or $\ln V$. It might be expected that $\ln \theta_1$ and $\ln \theta_3$ would vary linearly with $\ln V$ as does the Debye temperature for crystalline solids. This was not, however, observed and may be related to an anomalous thermal expansion coefficient implied by the strong temperature dependence of dC_V/dP . The fractional increase in θ_1 with increasing pressure is only about 30 percent of that for θ_3 . This is not surprising in that θ_1 is associated with the linear nature of the polymer chain. It is reasonable that compression would have a greater effect on the interchain spacing or force constants than on the intrachain spacing.

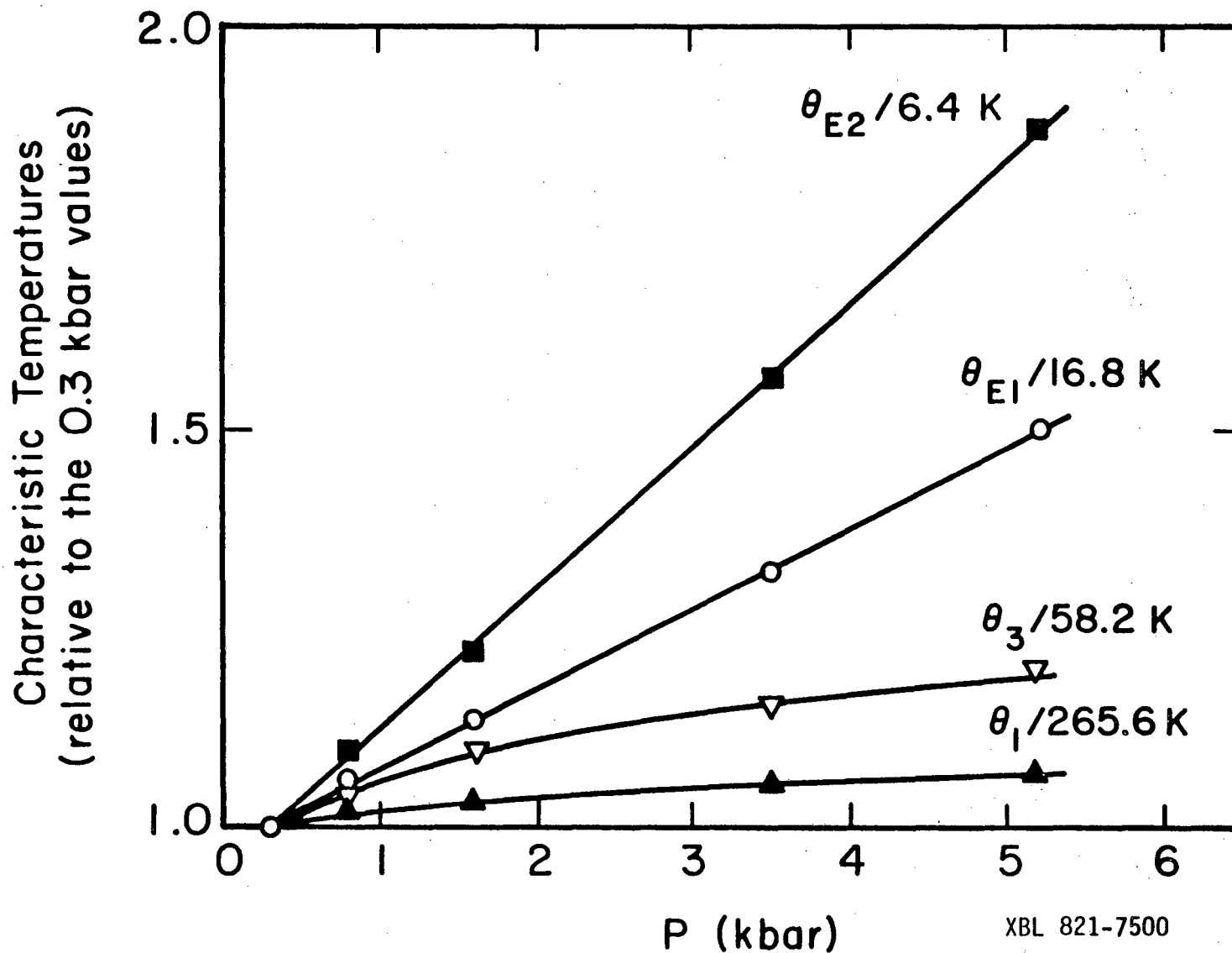


Fig. 4. The variation of the two Einstein characteristic temperature θ_{E1} and θ_{E2} and the two Tarasov characteristic temperatures θ_1 and θ_3 with pressure relative to their 0.3kbar values.

Table I. Parameters obtained by fitting the heat capacity of teflon to a Tarasov model plus two Einstein oscillator contributions.

P (kbar)	C/T^3 $T=0$ (mJ/mole-K ⁴)	θ_1 (K)	θ_1 (K)	θ_{E1} (K)	θ_{E2} (K)
0.3	2.88	265.6	58.2	16.8	6.4
0.8	2.62	269.3	60.6	17.5	7.0
1.6	2.34	273.0	63.7	19.0	7.8
3.5	2.08	279.2	66.8	22.2	10
5.2	1.88	282.9	69.8	25.2	12

The two Einstein temperatures θ_{E1} and θ_{E2} at 0.3kbar (16.8 and 6.4K) are very similar in magnitude to those found by Choy et al. for polymethyl methacrylate (PMMA) with θ_{E1} and θ_{E2} equal to 17.5 and 4.9K and for polystyrene (PS) with θ_{E1} and θ_{E2} equal to 16 and 5.5K.² The fraction of modes $n_1/4$ and $n_2/4$ associated with the C_{E1} and C_{E2} are also similar (0.75 and 0.036 percent for teflon, 1.8 and 0.038 percent for PMMA, and 1.0 and 0.014 percent for PS). The peaks in the phonon spectrum giving rise to the Einstein contributions to C_v are often associated with vibrations of certain groups near voids. Choy et al. correlate the smaller phonon peak (at θ_{E2} in the present notation) with vibrations of end units of the polymer chains by noting that about 0.1 percent of the repeat units are chain ends corresponding to about 0.025 percent of the vibrational modes.² They propose a model of pendant groups vibrating within voids to account for the larger phonon peak associated with C_{E2} . The similarity of θ_{E1} and n_1 for teflon, PMMA, and PS shows that this is an unreasonable interpretation. This follows from noting that teflon has no pendant groups to participate in such vibrations, but has a nearly identical heat capacity anomaly. Zoller et al. propose that the phonon peak of θ_{E2} may be the lowest-frequency normal mode of chain segments 35-50 repeats units in length.⁴ This idea is attractive in that no pendant groups are necessary. However, extension of this hypothesis to inorganic amorphous materials, in which similar heat capacity anomalies are seen, requires the existence of "microcrystallites" of about 100 masses. This seems unreasonable in that the vibrational frequency would depend

strongly on the details of sample preparation. Furthermore, it appears that the excess heat capacity would vanish in the limit of a completely amorphous specimen.

The present experiment, in which both crystallinity and chemical composition remain constant, shows that voids or free volume within amorphous regions are the most important factor in determining C_{EX} . Even though n_1 and n_2 are less than 1 percent of the total number of modes, their contribution to C_v is as large as 33 percent and they contribute more than 50 percent of the pressure dependence near the maximum in C/T^3 . Fits of the data show that n_1 and n_2 are pressure independent and that θ_{E1} (which is associated with the larger contribution to C_{EX}) increased by 50 percent at $P = 5.2$ kbar. While the degree of crystallinity (or the number of voids) has a large effect on the magnitude of C_{EX} in polymers, the characteristic temperature associated with the major contribution to C_{EX} is insensitive to crystallinity. From these observations, it is concluded that compression, which increases the amorphous packing density, increases the repulsive forces between chain segments within voids and leads to larger force constants or higher vibrational frequencies. The resulting picture is one in which polymer chains near voids are relatively free to vibrate perpendicularly to the linear dimension of the chain. Compression tends to close the voids leading to stiffer force constants and shifting the vibrations to higher frequency. It is reasonable that common features of polymers lead to voids of comparable size and that a particular void size is favored which would account for the sharply peaked

distribution of low frequency modes. For inorganic amorphous materials, the peaks in the phonon spectrum occur at higher frequencies and presumably reflects the greater structural differences between polymers and inorganic glasses than among polymers. The masses near voids would, however, be less constrained and it is possible that their vibrational frequencies would be strongly peaked leading also to an Einstein contribution to their heat capacity.

Note Added in Proff

Additional heat capacity measurements on teflon by Fisher, Van Curen, and Lasjaunias,¹⁶ at zero pressure and for which useful data extend down to 0.3K, have permitted a somewhat different analysis of the teflon data. These new results show that the parameters derived in this work are not as unique as was suggested by the sensitivity of the overall fits to variation of a single parameter. While the new analysis gives parameters varying by as much as 50 percent, the conclusions presented here are unchanged.

REFERENCES

1. R. P. Madding, D. L. Fehl, and J. R. Dillinger, *J. Polym. Sci. A-2*, 11, 1435 (1973).
2. C. L. Choy, R. G. Hunt, and G. L. Salinger, *J. Chem. Phys.* 52, 3629 (1970).
3. William Reese, *J. Appl. Phys.* 37, 3959 (1966).
4. P. Zoller, D. L. Fehl, and J. R. Dillinger, *J. Polym. Sci. A-2* 11, 1441 (1973).
5. C. L. Choy, W. Y. Leung, and F. C. Chen, *J. Polym. Sci. A-2* 17, 87 (1979).
6. J. E. Tucker and W. Reese, *J. Chem. Phys.* 46, 1388 (1967).
7. C. L. Choy, M. Huq, and D. E. Moody, *Phys. Lett. A* 54, 375 (1975).
8. W. Reese and J. E. Tucker, *J. Chem. Phys.* 43, 105 (1965).
9. V. V. Tarasov, *Zh. Fiz. Khim.* 24, 111 (1950).
10. Herbert B. Rosenstock, *J. Phys. Chem. Solids* 23, 659 (1962).
11. George P. Koo, *Fluoropolymers*, Leo A. Wall, ed. (Wiley-Interscience, New York), Chapter 16, 507.
12. R. C. Zeller and R. O. Pohl, *Phys. Rev. B* 4, 2029 (1971).
13. Bernhard Wunderlich, *J. Chem. Phys.* 37, 1203 (1962).
14. A. D. Athoughies, B. T. Peterson, G. L. Salinger, and C. D. Swartz, *Cryogenics* 6, 49 (1966).
15. Bernhard Wunderlich, *J. Chem. Phys.* 37, 1207 (1962).
16. R. A. Fisher, J. Van Curen, and J. C. Lasjaunias, to be published.

ACKNOWLEDGMENTS

I would like to thank Professor N. E. Phillips for suggesting the α -cerium work and for his guidance and advise during my tenure as a graduate student. Special thanks are also owed to Bill Fogle and Dr. Robert Fisher for their frequent and helpful discussion of low-temperature science and technology. Thanks are also due to Dr. Robert Fisher, John Van Curen, and Dr. J. C. Lasjaunias for sharing their recent zero pressure teflon heat capacity results. I also wish to thank John Van Curen, Mike Mayberry, Dr. Gary Brodale, and Dr. Erwin Hornung with whom I also had useful interactions.

Dr. Karl Gschneidner Jr., of Ames Laboratory, Iowa State University, collaborated with Professor Phillips and I on the cerium work and provided both the cerium samples and helpful communications. Duane Newhart of the Lawrence Berkeley Laboratory contributed to the early design stages of the high pressure cell. Nancy Monroe helped prepare the figures and Diana Morris helped prepare this manuscript.

Special thanks are due to Jeanette (Millard), my wife. Her support and encouragement played a vital role in the completion of this work.

This work was supported by the Director, Office of Energy Research, Office of Health and Environmental Research of the U.S. Department of Energy under Contract No. DE-AC03-76SF00098.

105
E 10

This report was done with support from the Department of Energy. Any conclusions or opinions expressed in this report represent solely those of the author(s) and not necessarily those of The Regents of the University of California, the Lawrence Berkeley Laboratory or the Department of Energy.

Reference to a company or product name does not imply approval or recommendation of the product by the University of California or the U.S. Department of Energy to the exclusion of others that may be suitable.

TECHNICAL INFORMATION DEPARTMENT
LAWRENCE BERKELEY LABORATORY
UNIVERSITY OF CALIFORNIA
BERKELEY, CALIFORNIA 94720